

# Spectroscopy of ultra-steep spectrum radio sources: a sample of $z > 2$ radio galaxies

H.J.A. Röttgering<sup>1,2,3</sup>, R. van Ojik<sup>1</sup>, G.K. Miley<sup>1</sup>, K.C. Chambers<sup>4</sup>, W.J.M. van Breugel<sup>5</sup>, and S. de Koff<sup>1,6</sup>

<sup>1</sup> Leiden Observatory, P.O. Box 9513, 2300 RA, Leiden, The Netherlands

<sup>2</sup> Mullard Radio Astronomy Observatory, Cavendish Laboratory, Madingley Road, Cambridge, CB3 0HE, England

<sup>3</sup> Institute of Astronomy, Madingley Road, Cambridge, CB3 0HA, England

<sup>4</sup> Institute for Astronomy, University of Hawaii, 2680 Woodlawn Drive, Honolulu, Hawaii 96822, USA

<sup>5</sup> Institute for Geophysics and Planetary Physics, Lawrence Livermore National Laboratory, L-413, Livermore, CA 94550, USA

<sup>6</sup> Space Telescope Science Institute, 3700 San Martin Drive, Baltimore MD 21218, USA

Received 12 December 1995 / Accepted 22 July 1996

**Abstract.** We present spectroscopic observations for 64 radio galaxies having ultra steep radio spectra. Twenty-nine objects have redshifts  $z > 2$ , the largest redshifts being almost 4. Our ultra steep spectrum (USS) criterion ( $\alpha < -1$ ) has proven to be the most efficient way of finding distant radio galaxies. We find that even among the USS sources, there is a strong statistical correlation between the spectral index and redshift. The most distant radio galaxies within the USS sample have the steepest radio spectra.

In our sample there are 3 radio galaxies at  $z > 3$  compared with 26 at  $2 < z < 3$ . However, the present data do not allow us to decide whether there is a decrease in co-moving source density at the highest redshifts.

We have analyzed the spectra of the 30 objects with the highest redshifts ( $z > 1.9$ ). For these high redshift radio galaxies,  $\text{Ly}\alpha$  is almost always the dominant emission line, with a rest frame equivalent width ranging from  $\sim 100 \text{ \AA}$  to more than  $1000 \text{ \AA}$ . The equivalent widths of the most important emission lines ( $\text{Ly}\alpha$ , C IV, He II, C III]) are found to correlate strongly with each other. The large rest frame equivalent widths and the correlation between the equivalent widths of the emission lines, confirm that photoionization by a central continuum source is most likely the dominant ionization mechanism.

There are significant velocity differences between the various emission lines of our high redshift radio galaxies; in particular the  $\text{Ly}\alpha$  line is shifted with respect to the higher ionization lines. Velocity shifts range from 100 to almost  $1000 \text{ km s}^{-1}$  in some cases. Simulations show that the effects of associated H I absorption on the  $\text{Ly}\alpha$  emission line may be responsible for most of these velocity shifts. However, other mechanisms such as organized kinematics of the  $\text{Ly}\alpha$  emission line gas (e.g. inflow or outflow) and obscuration of the line emission from the far side of the radio galaxy may also play a role.

**Key words:** galaxies: active – galaxies: redshifts – galaxies: ISM – radio continuum: galaxies

## 1. Introduction

The most distant observable galaxies are radio galaxies. Because these objects can be seen to large redshifts and because they are spatially extended, they are unique probes of the early Universe and important laboratories for testing models of galaxy formation. The most efficient way of obtaining significant samples of radio galaxies at redshifts  $z > 2$  is to concentrate on the counterparts of radio sources with ultra-steep spectra (USS,  $S \sim \nu^\alpha$ ,  $\alpha \lesssim -1.0$ ; e.g. Miley & Chambers 1989; Chambers & Miley 1989). During the last 5 years more than 60 radio galaxies with  $z > 2$  have been discovered (including those described in this paper), mostly using this technique. The most distant USS radio galaxy discovered so far is 8C1435+633 at  $z = 4.25$  (Lacy et al. 1994a).

High redshift radio galaxies (HZRGs) exhibit a large variety of properties. Remarkable is the initially unexpected alignment between the UV/optical emission and the radio structures and the common presence of enormous ( $> 100 \text{ kpc}$ ) ionized gas halos for which the Lyman  $\alpha$  emission line is very strong (e.g. McCarthy 1993). The variety of emission components from HZRGs and their large luminosities provide unique diagnostics for studying galaxies in the early Universe.

In order to study the nature of HZRGs and their evolution, it is important to obtain a large sample of such objects. After the initial success of the high redshift search technique on a sample of 4C USS sources (8 of 33 had  $z > 2$ , Miley & Chambers 1989; Chambers & Miley 1989), we set about increasing the number of HZRGs by extending the USS search method to larger and fainter samples of radio sources. The resultant

Leiden intermediate-flux compendium of USS sources was the basis for a key programme carried out at the European Southern Observatory in Chile between 1990 and 1994. This programme was remarkably successful, resulting in the discovery of 22 new radio galaxies with  $z > 1.9$ .

The project consisted of several steps. First, samples of USS sources were compiled having a range of finding frequencies and flux densities (see Röttgering et al. 1994). Secondly, high resolution ( $1.5''$ ) imaging of USS sources with the VLA was carried out (see Röttgering et al. 1994) to obtain good positions so that the USS sources could be identified on deep CCD images. Thirdly, a subset of the sources was imaged in  $R$  band with 2-m class telescopes to obtain reliable identifications (see Röttgering et al. 1996a). Finally, low-resolution spectroscopy was carried out with 4m-class telescopes on a subset of the objects to determine their redshifts. Here we present the results of this spectroscopy. We have augmented it with previously unpublished data from the original 4C sample in order to carry out some initial statistical analyses. The spectra presented here have been the starting point for several follow-up programmes to investigate various properties of HZRGs, some of which are discussed elsewhere in this paper.

The structure of this paper is as follows. In Sect. 2, we describe the sample selection and in Sect. 3 the observations and reduction of the data. The redshifts and spectra are presented in Sect. 4. We also analyze the properties of the emission lines in this section determining velocity shifts between the emission lines and searching for correlations with other properties of the radio galaxies. In Sect. 5 we discuss our results. We consider the efficiency of the USS technique for finding high redshift radio galaxies and briefly discuss the radio luminosity function of USS sources at high redshifts. Furthermore, we investigate a possible origin for the observed velocity shifts of  $\text{Ly}\alpha$  with respect to the higher ionization lines as being due to associated H I absorption systems. In Sect. 6 we summarize our results and conclusions.

Throughout this paper we assume a Hubble constant of  $H_0 = 50 \text{ km s}^{-1} \text{ Mpc}^{-1}$  and a deceleration parameter of  $q_0 = 0.5$ .

## 2. Samples

The sources whose optical spectroscopy we shall discuss here, have been selected either from the compendium of USS sources as compiled by Röttgering et al. (1994) or from the 4C sample of USS sources as presented by Tielens et al. (1979).

### 2.1. Leiden USS compendium

The Leiden compendium of USS radio sources (Röttgering et al. 1994) contains sources from a variety of radio catalogues, including the 8C at 38 MHz (Rees 1990), the 6C at 151 MHz (Hales et al. 1988), the Texas Sky Survey at 365 MHz (Douglas et al. 1980), the Molonglo Catalogue at 408 MHz (Large et al. 1981), the 1400 MHz NRAO Sky Survey Condon (Condon & Broderick 1985; Condon & Broderick 1986) and the 4.85 GHz Sky Survey (Condon et al. 1989). The resulting compendium

therefore contains sources with a range of finding frequencies. The median flux density at 365 MHz is  $\sim 1 \text{ Jy}$ . A large fraction of the sources from this compendium has been imaged at  $R$ -band to a level of  $R > 24$  using 2-m class telescopes at ESO and La Palma (e.g. Röttgering et al. 1996a).

Since our main aim was to obtain a sample of  $z > 2$  radio galaxies for subsequent detailed studies, we selected sources for spectroscopy so as to optimize the chance of finding high redshift objects. In carrying out the project, compromises had to be made in the selection of targets. It was regarded as of paramount importance to increase the number of high redshift radio galaxies. In order to optimize the use of the scarce 4m-class telescope time towards this goal, additional selection criteria were applied to reduce the number of spectroscopic targets. While recognizing that these additional criteria introduce complications on subsequent statistical analyses, we regarded it as more important at this stage to increase the number of high redshift galaxies whose properties could be studied in detail. Two additional radio-based criteria were therefore used in optimizing the spectroscopic targets for high redshift objects. First, we excluded the counterparts of diffuse radio sources. Diffuse (Fanaroff-Riley Class I, Fanaroff & Riley 1974) radio morphologies are known to be associated with relatively weak (nearby) radio sources. Secondly, we concentrated on the counterparts of smaller ( $< 20''$ ) radio sources. Taking account of the well-known correlation of radio angular size with redshift for quasars (Barthel & Miley 1988), only 25% of  $z > 2$  steep spectrum quasars have angular sizes  $> 10''$ . Hence, even if radio galaxies are systematically larger by a factor of 2, this criterion should exclude relatively few  $z > 2$  objects. Finally, a selection on optical magnitude from the CCD imaging was applied, concentrating on the objects with faint optical identifications ( $R > 21$ ) as the best candidates for distant radio galaxies.

#### 2.1.1. 4C USS sample

The 4C USS sample comprised 33 sources from Tielens et al. (1979) that have spectral indices  $\alpha < -1$  between 178 and 5000 MHz. Further details on the sample selection and observations can be found in Chambers & Miley (1989); Chambers et al. (1987) and Chambers et al. (1996a). Within this sample 8 have  $z > 2$  (Chambers et al. 1996b), including 4C40.36 at  $z = 2.3$  (Chambers et al. 1988), 4C41.17 (Chambers et al. 1990) and 4C48.48 at  $z = 2.3$  (Chambers & Miley 1989). Here we will present the spectral properties for these 8 sources. Their median flux density at 365 MHz is  $\sim 2 \text{ Jy}$ .

## 3. Observations of the Leiden USS sample

The observations were carried out with CCD slit spectrographs on the 3.6m telescope and the NTT (3.5m) of the European Southern Observatory (ESO) at La Silla and on the WHT (4.2m) of the Observatorio del Roque de los Muchachos at La Palma. The ESO observations were carried out as part of a “Key Programme”. Details of the observational setup are given in Table 1. Typical observing times were 1–2 hours per object.

**Table 1.** Observational setup

Dates	Sep 90	Nov 90 May 91	Mar 91	Nov 91 Apr 92 Nov 92	Jan 92
Telescope	NTT	ESO 3.6	NTT	ESO 3.6	WHT
Instrument	EFOSC2	EFOSC	EMMI	EFOSC	ISIS
CCD	Thompson# 17	RCA # 8	Thompson	TEK # 26	EEV 4
CCD size	1024 <sup>2</sup>	1024 × 640	1100 × 1040	512 × 512	1280 × 1180
Binning	2 × 4	2 × 2	–	1 × 2	3 × 2
Binned Pixel	0.7	0.67''	0.44''	0.61''	0.74''
Slit	2.2''	2.5''	2''	2.5''	2.5''
Grism(s)/gratings	UV 300 / B300	B300	Grism 3	B300	R158B
Spectral ranges [ $10^3 \times \text{Å}$ ]	3.6 – 5.4 / 4.7 – 6.8	3.6 – 7	4.1 – 7.9	3.8 – 6.9	3.6 – 6.9
Wavelength resolution	25 Å	24 Å	18 Å	24 Å	20 Å

The emission line regions of distant radio galaxies are typically extended by at least several arc seconds and oriented along the radio axis (e.g. McCarthy et al. 1990b). In order to optimize the signal to noise for detecting such emission lines, we therefore usually aligned the slit in the direction of the radio source and used a relatively large slit width ( $> 2''$ ). The typical emission line widths of distant radio galaxies is  $\sim 1000 - 1500 \text{ km s}^{-1}$ . With the slit width and the gratings used (see Table 1), the resolution of the spectra are comparable to the expected width of the emission lines.

Since the targets were too faint to be seen on the TV guiders, the following procedure was used for positioning the objects in the slit. The slit was first centered on either a reference star from the Space Telescope Guide Star System (GSS) or from a star on the *R*-band CCD frames (Röttgering et al. 1996a), whose position had been accurately determined with respect to the GSS system. A short exposure was made to check that this fiducial star was indeed centered in the slit and the telescope was then offset to the target. Since the relative position between the target and the positional reference star is known with an uncertainty of less than  $0.5''$ , the target was assumed to be in the slit.

### 3.1. Reduction and analysis

Reduction of the spectra was carried out using the ‘Long-slit’ package in the IRAF image reduction package developed by the US National Optical Astronomy Observatory (NOAO). For the data taken on every night, first a bias was constructed averaging 10 “zero second” exposures taken at either the beginning or at the end of each night. This bias was subtracted from every non-bias frame. The pixel-to-pixel gains were calibrated using flat fields obtained from an internal quartz lamp. Wavelength calibration was carried out by measuring the positions on the CCD of known lines from either an He-Ne or a Cu-Ar calibration lamp, fitting a polynomial function to these data, and applying the resultant calibration factors. We estimate the accuracy of the wavelength calibration to be about 5% of the resolution, i.e.  $\sim 1 \text{ Å}$  (see Table 1).

The sky contribution was removed from the frames, by subtracting a sky spectrum obtained by fitting a polynomial to the intensities measured along the spatial direction on the two-dimensional spectrum not including the spatial rows/columns where the targets were positioned. One-dimensional spectra were extracted by averaging in the spatial direction over an effective aperture as large as the spatial extent of the brightest emission line. Each night one or two standard stars were observed and used for the flux-calibration. We estimate that the flux-calibration is good to  $\sim 10\%$ .

### 3.2. Identification procedure

After all the geometrical and intensity calibrations were applied and the sky background level was subtracted, identification of the various emission lines in the spectra was attempted.

Depending on their redshifts, the emission line spectra of radio galaxies are dominated by one or several of the following lines: Ly $\alpha$   $\lambda$  1216, [O II]  $\lambda$  3727, [O III]  $\lambda$  5007, H $\alpha$   $\lambda$  6563 + [N II]  $\lambda$  6583 (Spinrad 1986; Osterbrock 1989; McCarthy 1993). For the more distant ( $z > 1$ ) radio galaxies other lines that are characteristic of the spectra, but with fainter intensities (5–10% of Ly $\alpha$ ) are C IV, He II, C III], C II], [Ne IV], Mg II and [Ne V].

The procedure for determining the redshifts consisted of first attempting to identify detected emission lines with the dominant lines and thereafter searching for fainter lines at the appropriate redshift.

An additional consideration is the presence of the Ly $\alpha$  “break” in the continuum spectrum due to the Ly $\alpha$  forest or a decrease in the intensity of the stellar continuum bluewards of Ly $\alpha$ . The presence of such a break at the Ly $\alpha$ . The presence of such a break at the appropriate wavelength is an additional argument for identifying a line with Ly $\alpha$ .

We note that 1243 + 036 ( $z = 3.6$ ) is the only object in the  $z > 2$  sample for which we have detected only one emission line. For a number of reasons we are confident that the redshift is correct, the most important being that [O III] 5007 emission is clearly detected in the infrared at the expected wavelength (cf van Ojik et al. 1996).

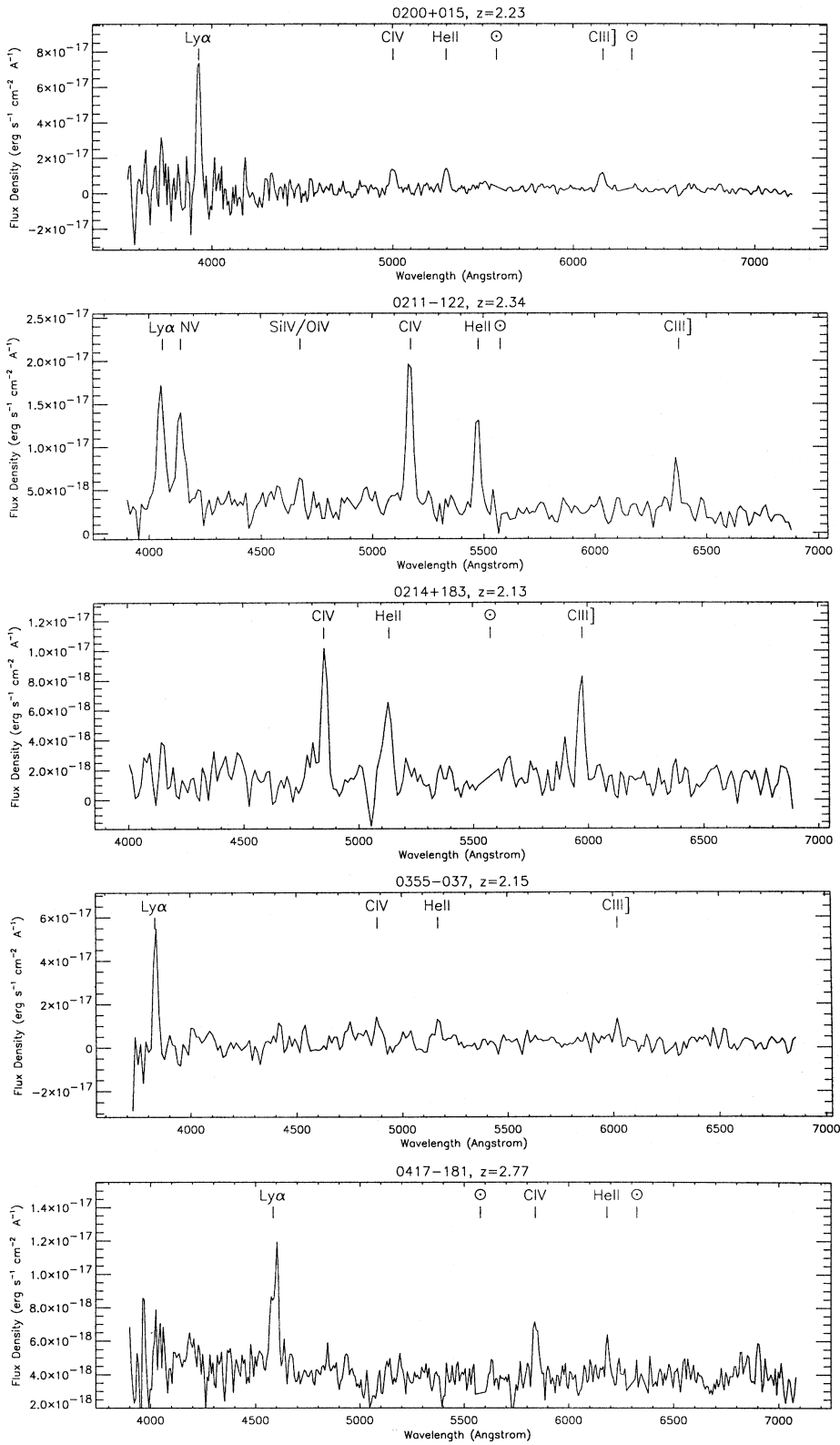


**Fig. 1.** One dimensional spectra of  $z > 1.9$  USS sources

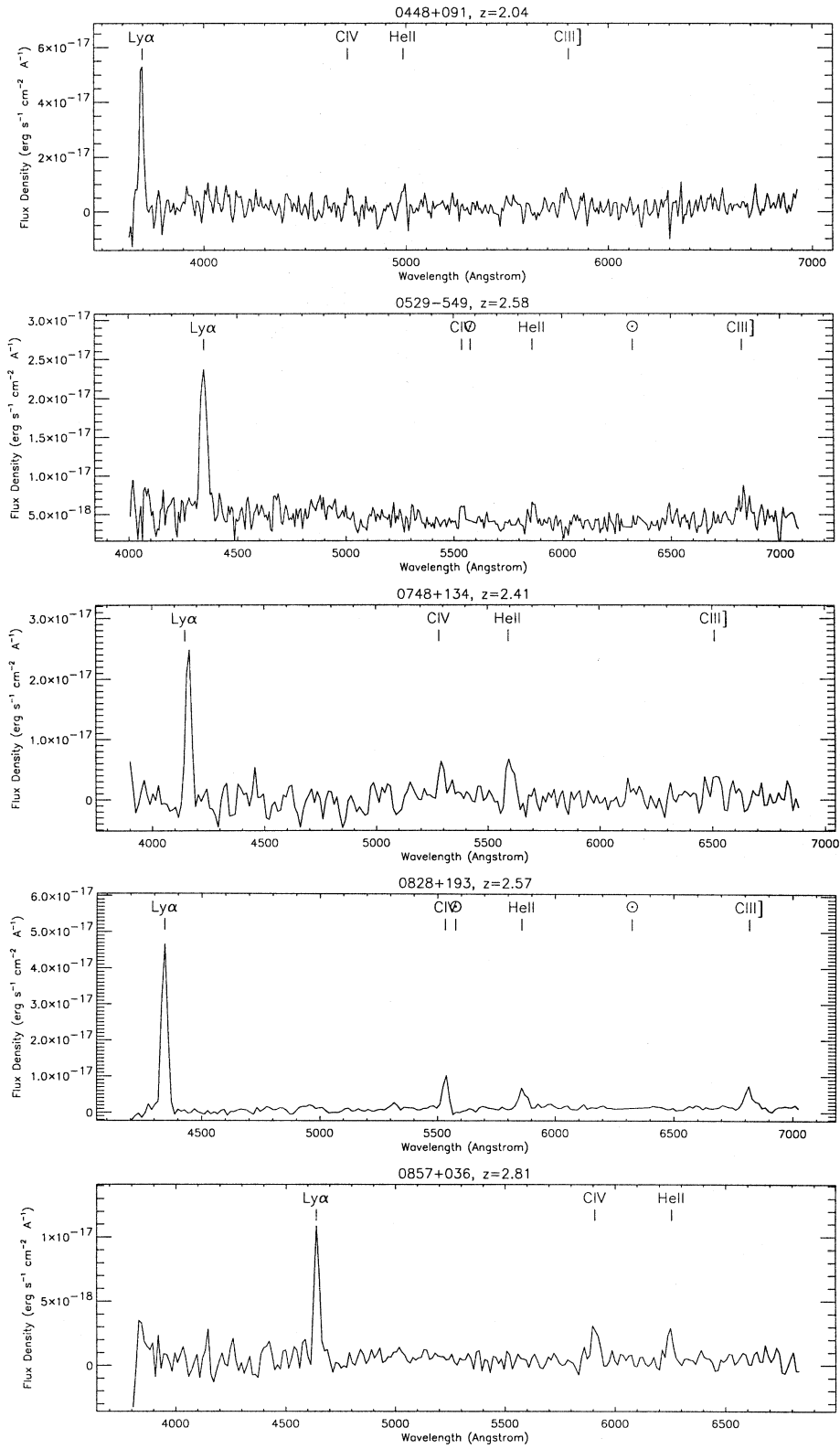


Fig. 1. (continued)

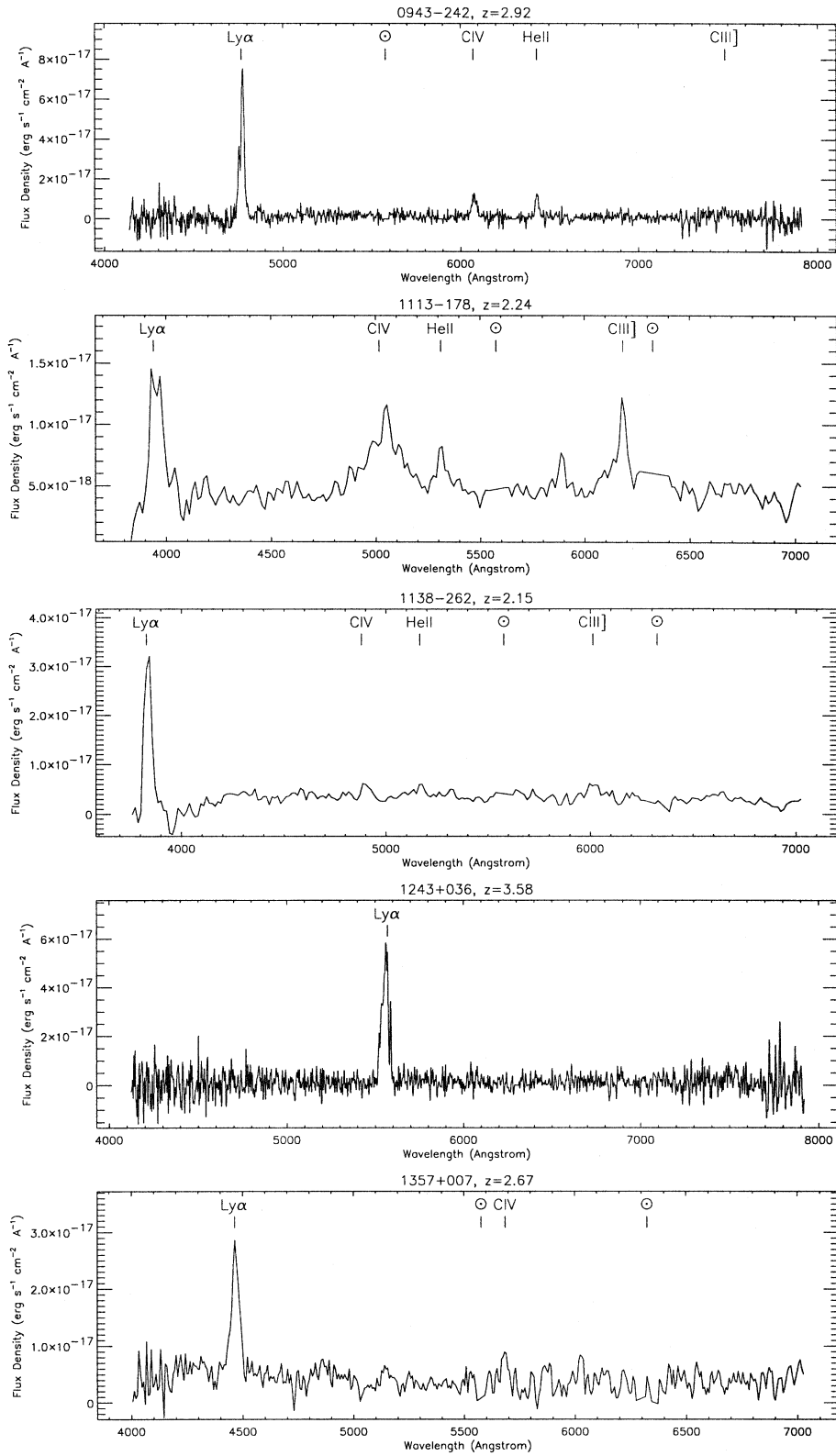


Fig. 1. (continued)

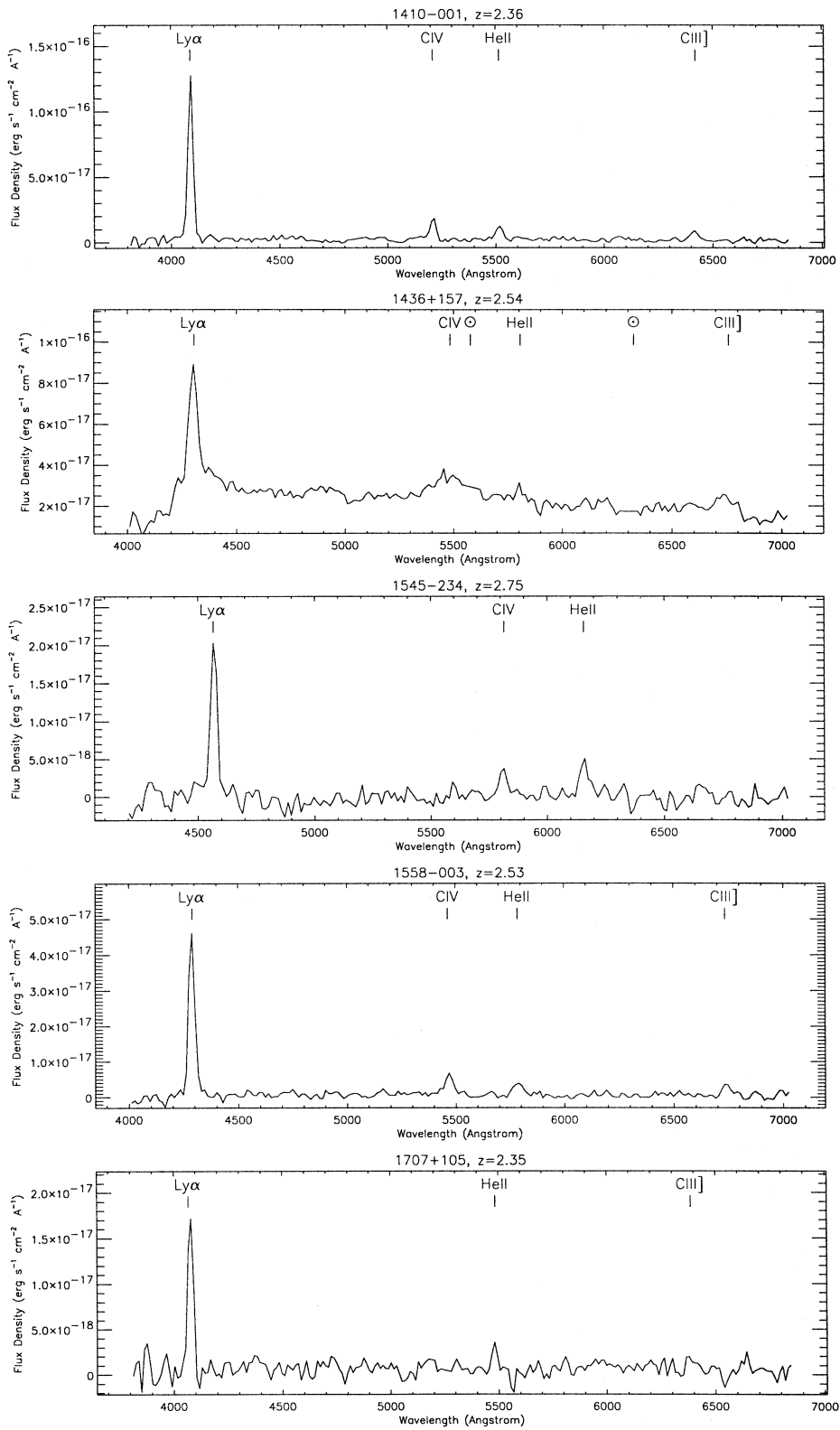


Fig. 1. (continued)

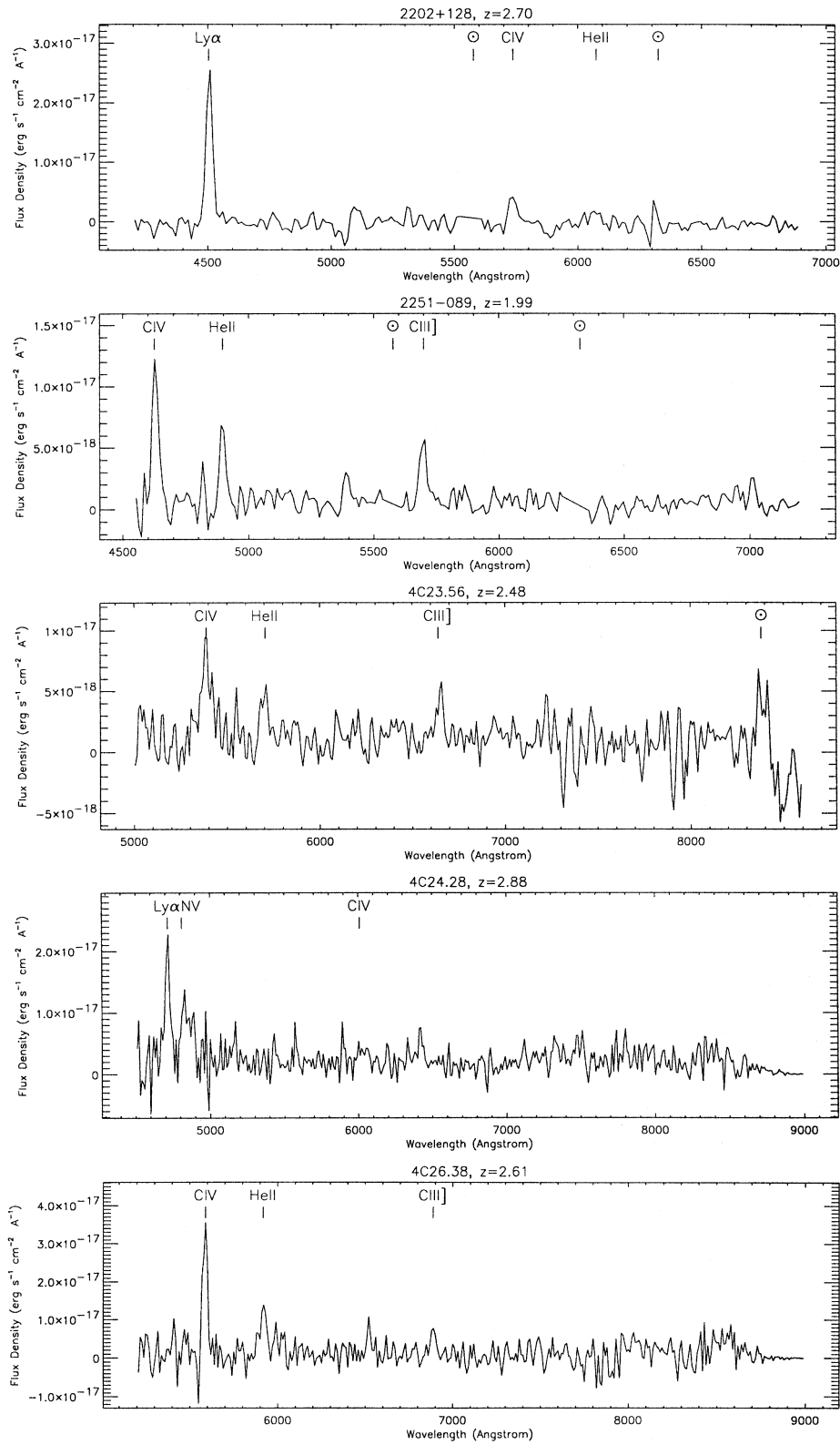


Fig. 1. (continued)

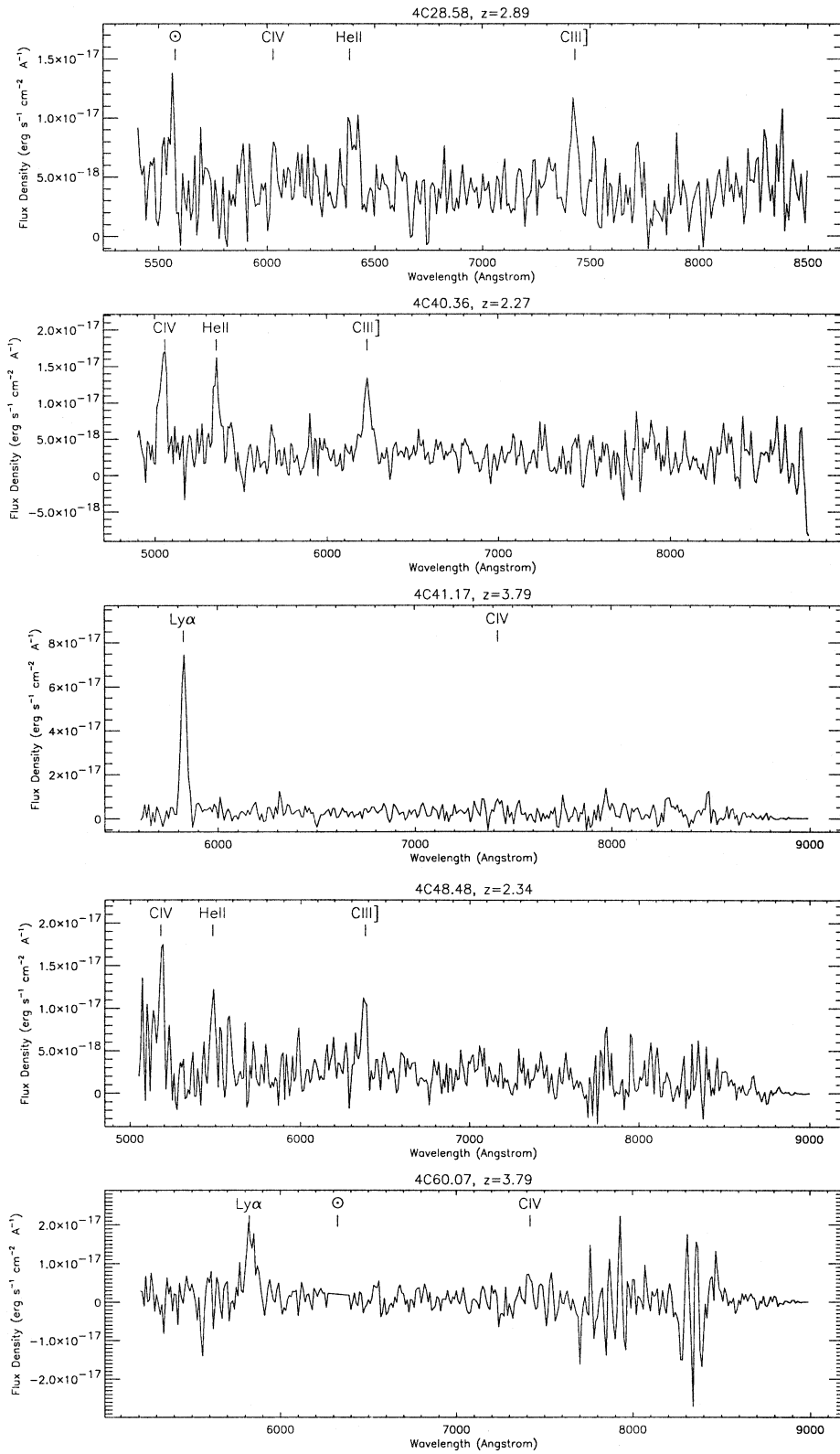


Fig. 1. (continued)

### 3.3. Analysis of the spectra

After an initial identification of the lines, each spectrum was analyzed and relevant parameters of the lines were determined. The first step was fitting the line with a Gaussian profile superimposed on a constant continuum. From this, the peak intensity and the width (FWHM) of the line were obtained.

The effect of noise on each spectrum was determined by calculating the RMS intensity in a line-free spectrum, i.e. excluding wavelengths within twice the measured FWHM of the emission lines or residual sky lines. The RMS intensities in these resulting spectra were calculated in bins of about 25 pixels. The values for the rms in each bin were fitted with 4th order polynomials. These polynomials then give an estimate of the local rms at each location in the spectra.

The uncertainty in the wavelength of the intensity peak of an emission line is a combination of the systematic uncertainties in the wavelength calibration, estimated to be 5% of the resolution, and the uncertainty in the measurement of the peak position, estimated to be  $(\text{FWHM} / (2s/n))$ , where  $s/n$  is the signal to noise ratio of the observed emission line (e.g. Condon 1989). The weighted average of the redshifts of the peaks of the emission lines has been taken as the redshift of the radio galaxies. The uncertainties in the redshift determination were calculated in two ways. First, it was calculated from a weighted average of the uncertainties in the peak positions of the identified lines. Secondly, it was calculated from the differences between the observed redshift of the source and the redshifts of the individual lines. Since some of the lines have velocity shifts with respect to other lines (see below) these two errors are not always in agreement. The uncertainty in the redshift, given in Table 2, is the largest of these two values. Especially the  $\text{Ly}\alpha$  emission line may be affected by H I absorption so that the true centroid of the  $\text{Ly}\alpha$  emission line is not well determined by a Gaussian fit. This may cause a different redshift for the  $\text{Ly}\alpha$  line than for the other emission lines in the spectrum (see Sects. 4.2 and 5.4), thus contributing to the uncertainty in the redshift.

The deconvolved widths (FWHM) of the lines were determined assuming that the lines are Gaussian. We note that from observations of the  $\text{Ly}\alpha$  emission at resolutions of a factor 10 higher than the observations presented here it is clear that the line profiles can be very complex (van Ojik et al. 1996, 1997). The deconvolved width presented here is therefore only a rough estimate of the true width. The formal uncertainty in the deconvolved width (FWHM) is a combination of (i) the uncertainty due to the signal to noise ratio of the line, estimated to be  $(\text{FWHM}/(s/n))$  (e.g. Condon 1989) and (ii) the uncertainty in the resolution, estimated to be 10%. If the fitted FWHM is less than its error, then the error in the deconvolved FWHM is taken as the upper-limit to the deconvolved FWHM.

The line flux was obtained by summing the intensities of the pixels above the determined continuum over a wavelength range of size 4 times the width (FWHM) of the line and centred at the peak of the emission line. The error in the flux determination is calculated taking into account (i) the signal to noise ratio of

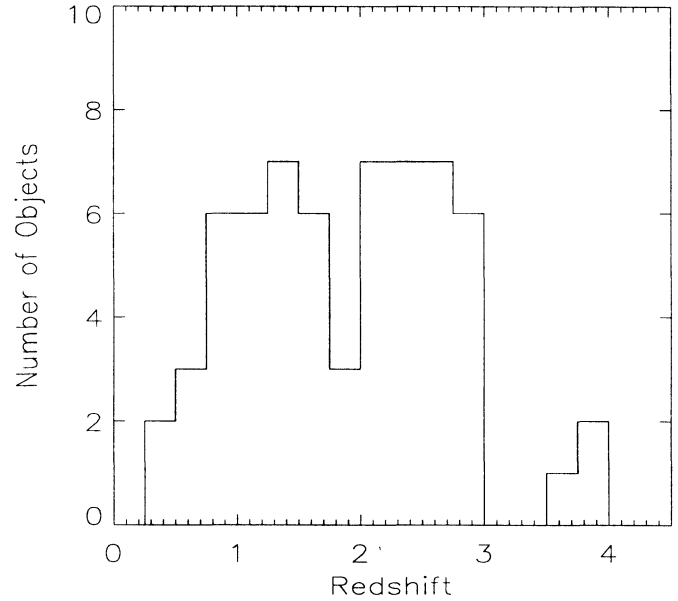


**Fig. 2.** Redshift distribution of the USS radio galaxies in our sample whose redshifts could be determined

the line and (ii) the error in the flux calibration, estimated to be 10%. We note that in general the emission region will be significantly more extended than the width of the slit and that therefore the fluxes of the lines are a lower limit to the total flux of the emission line.

The rest-frame equivalent width of each line was determined as the ratio of the line intensity to the local continuum intensity divided by  $(1+z)$ . Since the continuum emission from our targets is faint, in a significant number of cases only an upper limit to the continuum could be determined, yielding a lower limit to the equivalent width.

In general the spatial extent of the  $\text{Ly}\alpha$  emission line was observed to be significantly larger than the point spread function determined by the seeing. The angular size was determined by measuring the distance (in arcseconds) between the most extreme spatial points where  $\text{Ly}\alpha$  was detected on the two-dimensional spectrum, i.e. at a limiting surface brightness in the spectra of typically  $10^{-18} \text{ erg s}^{-1} \text{ cm}^{-2} \text{ \AA}^{-1} \text{ arcsec}^{-1}$ . This measurement is clearly dependent on parameters such as seeing and signal to noise ratio of the line and therefore the tabulated values should be taken only as an indication of the size. Furthermore, it is clear from narrow band imaging that the morphology of the  $\text{Ly}\alpha$  emission is usually complex and non-spherical. Hence, extensions in directions other than the slit direction (along the radio axis) will differ from the tabulated values presented here. The higher ionization lines were usually not detected with enough signal to noise to decide whether they were spatially resolved. They may be similarly extended as the optical continuum emission from the radio galaxies (usually  $2\text{--}3''$ ).

**Table 2.** Redshifts and emission line properties for  $z > 1.9$  objects

Name	$z$	Line	Peak Wavelength (Å)	Flux $10^{-16}$ (erg s $^{-1}$ cm $^{-2}$ )	FWHM (km s $^{-1}$ )	Eq. width (Å)	Ly $\alpha$ Extent (")
0200+015	2.229 $\pm$ 0.002	Ly $\alpha$	3927 $\pm$ 2	17.4 $\pm$ 2.2	< 681	> 256	6
		CIV	5002 3	4.2 0.5	1658 624	63 13	
		HeII	5297 2	3.2 0.4	890 506	36 5	
		CIII]	6158 2	4.0 0.5	1423 487	58 9	
0211–122	2.336 $\pm$ 0.002	Ly $\alpha$	4053 $\pm$ 1	5.7 $\pm$ 0.6	1698 $\pm$ 635	49 $\pm$ 6	10
		NV	4139 2	4.1 0.5	1812 666	35 4	
		SiIV/O	4674 6	0.6 0.2	< 736	5 2	
		CIV	5168 1	5.6 0.6	1225 472	48 5	
		HeII	5472 1	3.1 0.4	898 453	33 4	
		CIII]	6364 1	2.2 0.3	610 411	27 3	
0214+183	2.130 $\pm$ 0.003	CIV	4852 $\pm$ 1	3.0 $\pm$ 0.3	1142 $\pm$ 516	81 $\pm$ 12	
		HeII	5125 4	1.8 0.2	2016 586	50 8	
		CIII]	5971 2	1.8 0.2	801 423	38 5	
0355–037	2.153 $\pm$ 0.001	Ly $\alpha$	3836 $\pm$ 2	11.2 $\pm$ 1.8	< 667	> 263	8
		CIV	4883 4	2.7 0.6	859 690	26 7	
		HeII	5170 4	3.7 0.7	1514 687	62 18	
		CIII]	6018 3	2.3 0.5	< 470	33 9	
0417–181	2.773 $\pm$ 0.003	Ly $\alpha$	4594 $\pm$ 2	3.0 $\pm$ 0.3	2303 $\pm$ 590	17 $\pm$ 1	3
		CIV	5842 3	1.2 0.2	1047 510	8 1	
		HeII	6185 2	0.5 0.1	< 430	3 0	
0448+091	2.037 $\pm$ 0.002	Ly $\alpha$	3692 $\pm$ 1	12.2 $\pm$ 1.4	< 558	> 321	13
		CIV	4717 10	1.2 0.4	1542 885	> 101	
		HeII	4986 4	1.4 0.4	688 562	> 40	
		CIII]	5789 7	2.7 0.6	1709 930	> 60	
0529–549	2.575 $\pm$ 0.002	Ly $\alpha$	4345 $\pm$ 1	7.4 $\pm$ 0.8	1944 $\pm$ 591	39 $\pm$ 4	5
		CIV	5539 3	0.4 0.1	< 530	2 0	
		HeII	5866 3	0.6 0.1	< 524	4 0	
		CIII]	6833 10	1.8 0.3	2322 1047	11 1	
0748+134	2.419 $\pm$ 0.004	Ly $\alpha$	4161 $\pm$ 1	6.3 $\pm$ 0.8	1311 $\pm$ 503	> 522	5
		CIV	5292 3	1.8 0.3	1022 526	77 29	
		HeII	5598 5	1.5 0.3	1549 513	> 209	
		CIII]	6515 6	1.4 0.3	1293 671	> 62	
0828+193	2.572 $\pm$ 0.002	Ly $\alpha$	4342 $\pm$ 1	13.3 $\pm$ 1.3	1166 $\pm$ 548	> 2730	7
		CIV	5534 1	1.9 0.2	< 435	43 5	
		HeII	5862 2	1.9 0.2	1576 445	41 5	
		CIII]	6813 2	2.0 0.2	1261 378	39 4	
0857+036	2.814 $\pm$ 0.003	Ly $\alpha$	4640 $\pm$ 1	2.6 $\pm$ 0.3	1095 $\pm$ 441	113 $\pm$ 24	2
		CIV	5908 3	1.0 0.1	1650 426	78 17	
		HeII	6247 2	0.7 0.1	956 391	47 12	

## 4. Results

### 4.1. Redshifts

From our spectroscopic observations we have found redshifts for a total of 64 USS radio sources, of which 29 are at redshifts larger than 2. In Fig. 1 the individual spectra of the objects with  $z > 1.9$  are presented. The lines that we have identified are indicated in the plots of the spectra. We also have indicated with the symbol  $\odot$ , where the spectra are severely affected by

badly subtracted sky-lines. In a large fraction of such cases we excluded the affected pixels and therefore the residual sky-lines are absent on the plots of the spectra. In Table 2 the redshifts of the objects with  $z > 1.9$  plus the relevant parameters of the emission lines in the spectra are presented.

Table 3 lists the sources with redshifts smaller than 1.9. In the case of three objects for which only one emission line was detected, the redshift needs confirmation and is shown in parentheses. The redshift distribution of our sample of radio galaxies is shown in Fig. 2.

Table 2. (continued)

Name	$z$	Line	Peak Wavelength (Å)	Flux $10^{-16}$ (erg s $^{-1}$ cm $^{-2}$ )	FWHM (km s $^{-1}$ )	Eq. width (Å)	Ly $\alpha$ Extent (")
0943–242	2.923 $\pm$ 0.002	Ly $\alpha$	4772 $\pm$ 0	20.1 $\pm$ 2.0	1666 $\pm$ 264	> 653	3
		CIV	6076 2	3.9 0.4	1619 348	113 37	
		HeII	6430 1	2.7 0.3	874 241	83 29	
		CIII]	7478 8	2.3 0.4	1397 1053	> 91	
1113–178	2.239 $\pm$ 0.003	Ly $\alpha$	3953 $\pm$ 6	6.4 $\pm$ 0.7	5021 $\pm$ 764	51 $\pm$ 3	
		CIV	5042 62	1.7 0.4	10196 1530	8 1	
		HeII	5310 3	0.7 0.2	< 559	3 0	
		CIII]	6180 2	2.8 0.3	1708 459	16 1	
1138–262	2.156 $\pm$ 0.004	Ly $\alpha$	3837 $\pm$ 2	13.9 $\pm$ 1.6	2603 $\pm$ 695	> 832	
		CIV	4900 6	0.8 0.2	1982 728	6 1	
		HeII	5166 6	1.3 0.2	2787 1005	10 1	
		CIII]	6017 24	1.3 0.3	4285 1341	12 2	
1243+036	3.570 $\pm$ 0.001	Ly $\alpha$	5556 $\pm$ 1	23.5 $\pm$ 2.4	2454 $\pm$ 251	351 $\pm$ 13	7
1357+007	2.673 $\pm$ 0.002	Ly $\alpha$	4467 $\pm$ 1	9.1 $\pm$ 1.0	2188 $\pm$ 571	45 $\pm$ 4	3
		CIV	5682 5	1.7 0.3	957 653	13 2	
1410–001	2.363 $\pm$ 0.001	Ly $\alpha$	4089 $\pm$ 1	32.0 $\pm$ 3.2	1266 $\pm$ 485	356 $\pm$ 57	10
		CIV	5209 1	5.2 0.6	1330 402	78 11	
		HeII	5516 2	3.6 0.4	1617 430	48 7	
		CIII]	6413 3	3.3 0.4	1838 444	73 13	
1436+157	2.538 $\pm$ 0.003	Ly $\alpha$	4302 $\pm$ 3	42.0 $\pm$ 4.7	3731 $\pm$ 733	48 $\pm$ 5	8
		CIV	5474 44	17.0 1.9	9174 1397	19 2	
		HeII	5799 9	6.0 0.8	2952 998	8 1	
		CIII]	6730 42	9.4 1.7	4531 1956	16 2	
1545–234	2.755 $\pm$ 0.002	Ly $\alpha$	4567 $\pm$ 1	6.7 $\pm$ 0.7	1377 $\pm$ 534	> 900	5
		CIV	5810 4	1.1 0.2	1221 562	94 40	
		HeII	6158 4	1.8 0.3	1729 560	> 86	
1558–003	2.527 $\pm$ 0.002	Ly $\alpha$	4287 $\pm$ 1	14.9 $\pm$ 1.5	1529 $\pm$ 556	1180 $\pm$ 510	6
		CIV	5468 2	2.7 0.3	1965 501	95 15	
		HeII	5785 5	1.7 0.2	2468 613	82 17	
		CIII]	6739 4	1.2 0.2	1389 525	73 21	
1707+105	2.349 $\pm$ 0.005	Ly $\alpha$	4076 $\pm$ 1	4.3 $\pm$ 0.5	1466 $\pm$ 501	242 $\pm$ 80	16
		HeII	5480 3	0.9 0.2	972 475	70 24	
		CIII]	6384 22	0.2 0.1	1692 940	> 7	
2202+128	2.706 $\pm$ 0.001	Ly $\alpha$	4506 $\pm$ 1	7.7 $\pm$ 0.8	1167 $\pm$ 532	> 1375	3
		CIV	5736 5	1.9 0.4	1464 693	> 225	
		HeII	6064 14	2.4 0.5	3023 2071	> 309	
2251–089	1.986 $\pm$ 0.002	CIV	4628 $\pm$ 2	3.3 $\pm$ 0.4	985 $\pm$ 578	> 148	
		HeII	4895 2	1.3 0.2	< 549	66 19	
		CIII]	5696 2	1.5 0.2	1016 498	84 20	

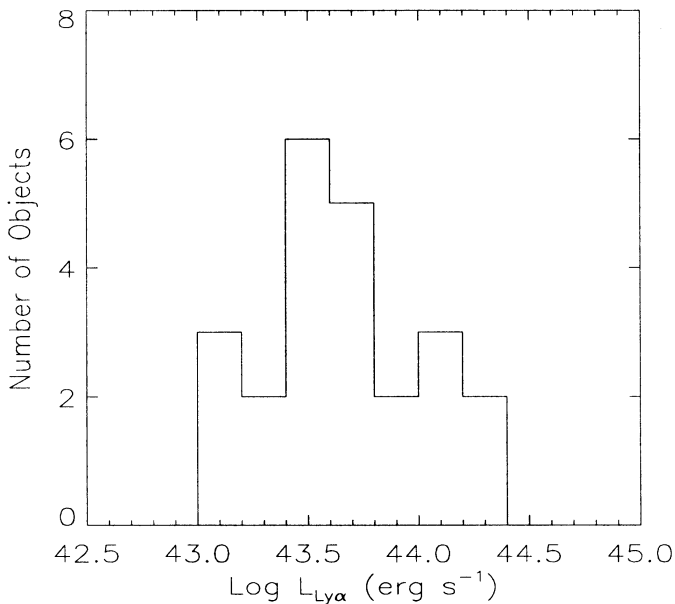
From a few objects broad emission lines were observed ( $> 4000$  km s $^{-1}$  FWHM) and they are therefore probably quasars. The broad line objects with  $z > 2$  are 1113-178 and 1436 + 157. The latter object is a quasar with a possible companion galaxy within the extended Ly $\alpha$  halo of the quasar, oriented along the radio axis. Because no obvious line emission was detected from the companion, we cannot definitely say whether this is an associated quasar-galaxy pair.

Statistical evidence for the preferential occurrence of companion galaxies in the direction of the radio axis was provided by

the  $R$  band images of our sample of radio sources (Röttgering et al. 1996a,b). However, line emission was usually observed only from one of both objects, as in the case of 0828 + 193 at  $z = 2.572$  and the above mentioned 1436 + 157 at  $z = 2.538$ . Therefore for these individual cases it is unclear whether both objects are at the same redshift. Only in 1707 + 105 at  $z = 2.349$  is the Ly $\alpha$  emission observed to have two clear spatial peaks corresponding to the  $R$  band positions of two galaxies oriented along the radio axis.

**Table 2.** (continued)

Name	z	Line	Peak Wavelength (Å)	Flux $10^{-16}$ (erg s $^{-1}$ cm $^{-2}$ )	FWHM (km s $^{-1}$ )	Eq. width (Å)	Ly $\alpha$ Extent (")
4C23.56	2.483 $\pm$ 0.003	CIV	5388 $\pm$ 10	5.1 $\pm$ 0.6	3695 $\pm$ 1020		149 $\pm$ 38
		HeII	5700 10	1.3 0.3	1636 896	31 8	
		CIII]	6651 4	1.5 0.3	734 626	34 8	
4C24.28	2.879 $\pm$ 0.006	Ly $\alpha$	4714 $\pm$ 3	7.3 $\pm$ 1.0	< 762		72 $\pm$ 12 5
		NV	4835 12	6.9 1.1	3562 2149	70 19	
		CIV	6028 24	1.7 0.4	3284 2610	20 6	
4C26.38	2.608 $\pm$ 0.001	CIV	5587 $\pm$ 2	8.9 $\pm$ 1.1	< 560		> 156
		HeII	5919 4	5.7 0.8	1367 734	116 46	
		CIII]	6888 5	2.4 0.5	< 603		> 45
4C28.58	2.891 $\pm$ 0.004	CIV	6033 $\pm$ 10	0.3 $\pm$ 0.2	< 615		> 1
		HeII	6399 14	1.6 0.4	2186 1007	9 2	
		CIII]	7424 5	1.8 0.4	569 520	12 2	
4C40.36	2.265 $\pm$ 0.003	CIV	5048 $\pm$ 4	6.2 $\pm$ 0.8	2017 $\pm$ 782		54 $\pm$ 9
		HeII	5356 3	5.6 0.7	1640 718	54 9	
		CIII]	6235 5	5.9 0.6	2370 668	67 10	
4C41.17	3.792 $\pm$ 0.001	Ly $\alpha$	5827 $\pm$ 1	22.0 $\pm$ 2.3	597 $\pm$ 514		159 $\pm$ 31 11
		CIV	7422 14	1.0 0.5	< 685		> 4
4C48.48	2.343 $\pm$ 0.003	CIV	5183 $\pm$ 3	6.1 $\pm$ 0.9	< 723		56 $\pm$ 13
		HeII	5485 4	3.7 0.6	< 766		44 11
		CIII]	6376 3	2.8 0.4	< 531		26 4
4C60.07	3.788 $\pm$ 0.004	Ly $\alpha$	5831 $\pm$ 9	10.1 $\pm$ 1.3	2875 $\pm$ 937		153 $\pm$ 71 7
		CIV	7412 6	2.7 0.8	< 740		> 90

**Fig. 3.** Distribution of the Ly $\alpha$  luminosities

#### 4.2. Emission line properties

In the following we shall investigate the properties of the emission lines and the presence of correlations between the derived

emission lines properties of the radio galaxies with redshifts larger than 1.9 (all objects from Table 2). We do not include the two objects with broad ( $> 4000$  km s $^{-1}$  FWHM) emission lines in the analysis. Thus, the sample for which we search for correlations of the properties consists of 28 HZRGs.

##### 4.2.1. Ly $\alpha$ properties

Ly $\alpha$  is the strongest and most spatially extended emission line in the spectra of our HZRGs. The measured spatial extent of Ly $\alpha$  along the slit ranges from a few arcseconds to 16 arcseconds, corresponding to  $\sim 25$  to 140 kpc. In Fig. 3 we show the distribution of Ly $\alpha$  luminosities. The large spatial extent of Ly $\alpha$  along the slit indicates that the Ly $\alpha$  extent perpendicular to the slit may be larger than the slit width ( $\sim 2.5''$ ). Therefore, it is possible that the true Ly $\alpha$  luminosities are a factor of  $\sim 2$  higher than measured in our spectra.

Roughly 80% of the radio galaxies have Ly $\alpha$  luminosities larger than  $10^{43.5}$  erg s $^{-1}$ . Given the sensitivities of our spectroscopy (see Röttgering 1993), this is unlikely to be a selection effect. The Ly $\alpha$  luminosities are comparable to the radio luminosities of the radio galaxies and also comparable to the luminosities of extended Ly $\alpha$  emission observed in high redshift radio loud quasars (Heckman et al. 1991).

Assuming a volume filling factor of the emission line gas of  $10^{-5}$  as derived from sulphur emission lines of low redshift radio

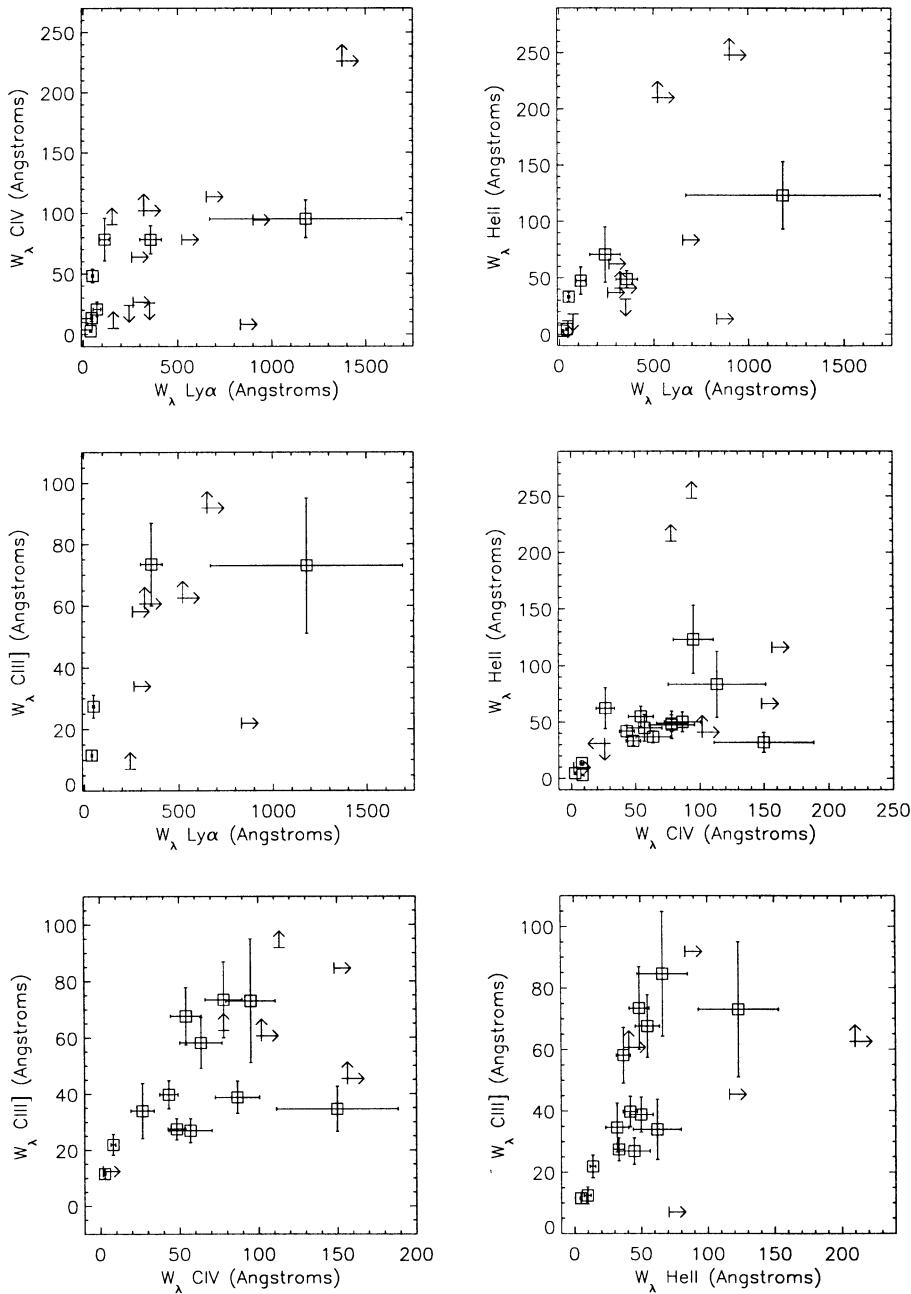


**Fig. 4.** The rest frame equivalent widths of the emission lines Ly $\alpha$ , C IV, He II and C III] plotted against each other. Lower limits are indicated in the plot as upward and rightward pointing arrows, upper limits as downward and leftward pointing arrows

galaxies (van Breugel et al. 1985; Heckman et al. 1982), the Ly $\alpha$  luminosities of the radio galaxies imply masses in ionized gas of a few times  $10^7$  to a few times  $10^8 M_{\odot}$  (see also van Ojik 1996 and 1997).

#### 4.2.2. Equivalent widths

The equivalent widths of the various emission lines (Ly $\alpha$ , C IV, He II, C III]) are plotted against each other in Fig. 4. In the cases where the continuum level could not be measured, lower limits to the equivalent widths were determined. In a few cases where an emission line was not detected but the continuum could be measured, an upper limit to the equivalent width of the line was determined.

We find that the rest frame equivalent widths of all 4 lines are strongly correlated with each other. Spearman rank analysis of the correlations give confidence levels of more than 99%. The strongest and most obvious correlations are visible between the equivalent widths of the higher ionization lines (C IV, He II, C III]). The correlations with the Ly $\alpha$  equivalent width are less significant.

We note that most of the lower limits imply that the true correlations between the equivalent widths might be even stronger than seen in Fig. 4. We found no evidence for correlations of the equivalent widths with other properties of the radio galaxies within our sample (radio size, luminosity, distortion, spectral index).

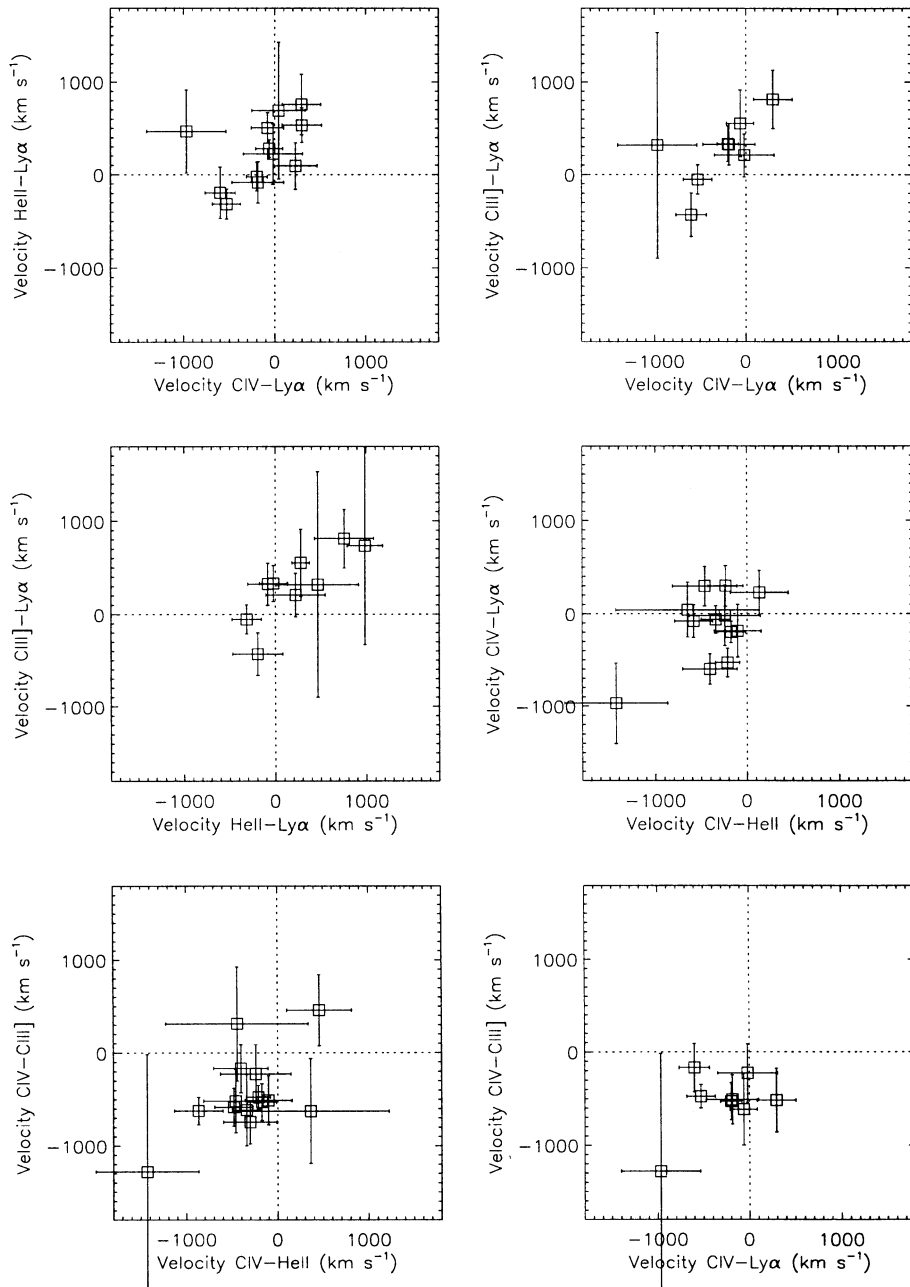


**Fig. 5.** The velocity shifts between the emission lines  $\text{Ly}\alpha$ , C IV, He II and C III] plotted against each other

#### 4.2.3. Velocity shifts between emission lines

In many cases we find that the redshifts of the peak intensities determined using Gaussian fits to the individual emission lines in a spectrum differ by more than the combined errors in the redshifts of the individual lines. The rms-uncertainties in the wavelength calibration are typically less than  $2 \text{ \AA}$ , corresponding to  $\sim 130 \text{ km s}^{-1}$ , while the measured velocity shifts between the lines are between several hundreds and sometimes almost  $1000 \text{ km s}^{-1}$ .

To establish the reality of these shifts we must ensure that there are no systematic errors in our wavelength determination. An uncertain wavelength determination may occur when an emission line occurs at a wavelength outside the range of the

lines emitted by the calibration lamp, so that the wavelengths are determined by extrapolation rather than by interpolation from the calibration lines. This is the case for 0448+091, where  $\text{Ly}\alpha$  is at  $3692 \text{ \AA}$  and the detections of C IV, He II and C III] are marginal. In the observing session during which 0448+091 was observed (WHT January 1991) there were few calibration lines in the far blue. The bluest usable calibration line was at  $4131 \text{ \AA}$ . Thus, the  $\text{Ly}\alpha$  emission line was  $340 \text{ \AA}$  blueward of the nearest calibration line. This extrapolation may well have caused an erroneous determination of the wavelength of  $\text{Ly}\alpha$  and we therefore ignore this galaxy in considering the velocity correlations. During the other observing sessions there were no such problems and calibration lines were available down to  $3888 \text{ \AA}$ .

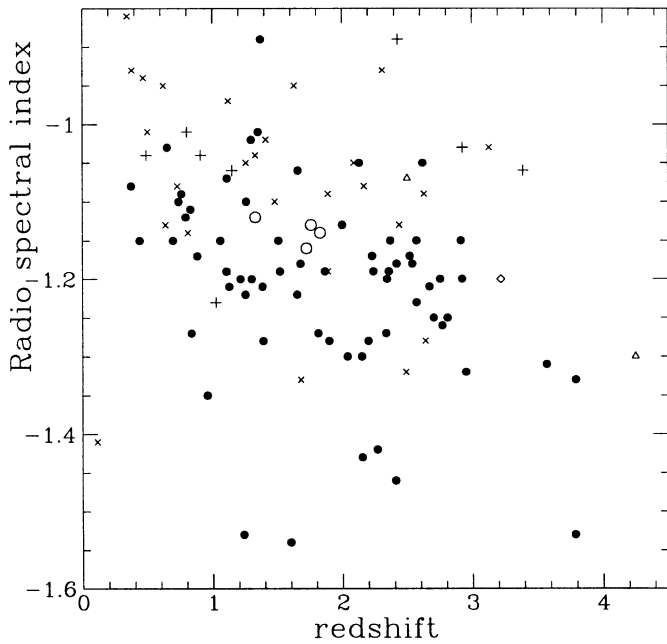


**Fig. 6.** Radio spectral index plotted against redshift for 108 radio galaxies. Filled dots are from our USS sample. The spectral indices are determined between the lowest available frequency above 150 MHz and 5 GHz. The open circles are also from our USS sample with redshifts obtained at Lick Observatory by McCarthy & van Breugel (1994, private communication). The crosses (×) are from the Molonglo sample of McCarthy (1990a, 1990b), the pluses (+) are Bologna sources (McCarthy 1991, Lilly 1988), the triangles are from the 8C survey (Lacy et al. 1994, Lacy 1992) and the diamond is 6C 1232 + 39 (Eales & Rawlings 1993)

Finally, there is the problem is the presence of strong sky-lines. In the objects 0529 – 549, 0828 + 193 and 4C 26.38 the C IV emission line is affected by the 5577 Å skyline. We have therefore excluded these three objects in the following analysis of the velocity shifts.

After also leaving out 1243 + 036 for which Ly $\alpha$  was the only detected emission line in the spectrum, the final sample for which we have carried out the velocity shift analysis consists of 23 HZRGs. The determined velocity shifts between the various emission lines and their uncertainties are listed in Table 4. In this table negative values indicate that the first line is redshifted with respect to the second. Although the uncertainties on most velocity shifts are large and the shifts have only a 2–3  $\sigma$  significance, the presence of velocity shifts in the sample is statistically significant (see below).

In Fig. 5 we show the velocity shifts between the emission lines Ly $\alpha$ , C IV, He II and C III] plotted against each other. Several correlations between the velocity differences are apparent: strong correlations are present between the measured velocity differences of the higher ionization lines with respect to Ly $\alpha$ . Objects with larger velocity shifts in one high ionization line with respect to Ly $\alpha$  tend to show also larger shifts of the other high ionization lines with respect to Ly $\alpha$ . This is strong evi-

**Table 3.** Redshifts of objects from the Leiden USS compendium with  $z < 1.9$

Name	$z$	Session	Comments
0008+172	1.390	nov90	
0036+205	1.370	aug90	
0050+204	1.297	aug90	
0054+090	1.301	nov91	
0203–478	0.836	nov93	
0241+348	1.215	aug90	
0255+114	(0.447)	jan92	
0256+324	(1.657)	dec89	
0324–228	1.898	jan91	
0338–259	0.440	nov93	
0410–198	(0.793)	nov91	
0429–267	1.26	nov91	
0447–164	1.814	nov90	
0548–150	0.650	nov93	
0729–722	0.738	nov91	
0819+672	0.760	jan91	
0850+140	1.106	jan92	Quasar
1035+208	0.696	may91	
1043–216	1.060	mar91	
1104+089	1.384	jan92	
1228–166	1.127	jan92	Quasar
1238–273	1.253	may91	
1449–004	1.466	may91	
1502+039	1.652	may91	
1548–111	0.959	apr92	
1635+396	1.600	jul91	
1657+003	1.110	may91	
1725+167	1.508	may91	
2000–091	1.238	may91	
2214+134	0.374	aug90	
2224–273	1.678	sep90	
2226+162	1.519	nov91	
2245+181	0.830	aug90	
2339+269	0.882	aug90	

dence that there is a real systematic shift between the redshift of the peak intensity of Ly $\alpha$  with respect to the other lines.

From Fig. 5 it can also be seen that in almost all objects C IV is redshifted with respect to both He II and C III]. The average shift of C IV with respect to He II is  $-332 \pm 101 \text{ km s}^{-1}$  and C IV with respect to C III] is  $437 \pm 125 \text{ km s}^{-1}$ . There may also be a correlation between the velocity differences of C IV with He II and C IV with C III], although the errors on the individual points of the plot are larger than in the case of the first three correlations.

One object that has a relatively large offset in the plots from the other objects and relatively large uncertainties is 1138 – 262. This radio galaxy is a very peculiar galaxy, both from its  $R$  band image, where it is an extremely clumpy galaxy (Pentericci et al. 1997), and from a high resolution radio image (Carilli et al. 1997), where it appears as a string of radio knots. Furthermore, the high resolution Ly $\alpha$  spectrum reveals that it has a very peculiar velocity structure (Pentericci et al. 1997). Although it has these peculiarities which may be the cause of its particular po-

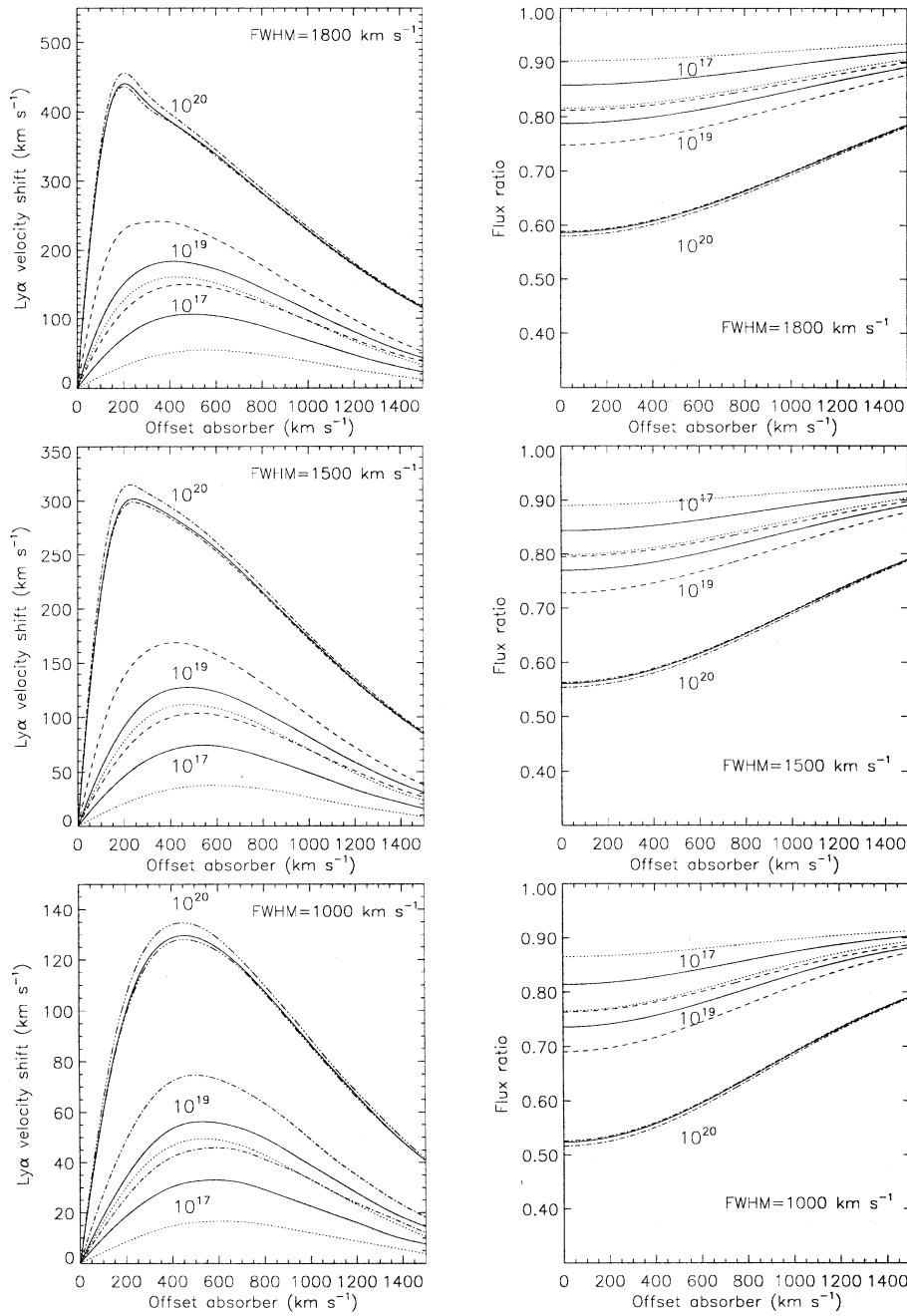


**Fig. 7.** *Left*) Velocity shifts of observed Ly $\alpha$  peaks produced by H I absorption systems as a function of absorber offset velocity. Plots are for different  $N(\text{H I})$  as indicated (in  $\text{cm}^{-2}$ ). Solid lines are for  $b = 50 \text{ km s}^{-1}$ , dashed/dotted lines are lower and upper values calculated for  $b = 25$  and  $75 \text{ km s}^{-1}$ . *Right*) Flux ratios of Ly $\alpha$  before and after absorption with indicated H I column density. Solid lines for  $b = 50 \text{ km s}^{-1}$  lower and upper dashed/dotted lines for  $b = 75$  and  $25 \text{ km s}^{-1}$ . For more details see text

sition in the velocity plots, we have no reason to believe that our velocity determination has any systematic error as in the case of 0448+091.

We find from a Spearman rank analysis that the correlations of velocity shifts of the higher ionization with respect to Ly $\alpha$  are significant at a confidence level of more than 99%. The apparent (C IV–He II)–(C IV–C III)] correlation would have a formal significance in a Spearman rank analysis of 95%, but the errors on the individual points are too large to allow a Spearman rank analysis. Furthermore, if the previously mentioned radio galaxy 1138 – 262 is omitted, the correlation becomes insignificant (85%). Thus, we conclude that this apparent correlation is not statistically significant. No significant correlations were

found between the other velocity differences. Thus, the three most significant correlations in the velocity shifts indicate that there is frequently a velocity shift between the Ly $\alpha$  line and the higher ionization lines.

Summarizing, we find that in many cases significant velocity shifts between emission lines are present. Velocity shifts of Ly $\alpha$  with higher ionization lines are strongly correlated and C IV appears to be mostly redshifted with respect to He II and C III]. A comparison with velocity shifts earlier reported in quasars and radio galaxies (Gaskell 1982; Wilkes 1984; Espey et al. 1989; Corbin 1990; Carswell et al. 1991; McCarthy et al. 1990a; Tadhunter 1991; Eales et al. 1993b) and their possible interpretation will be discussed in a next section.

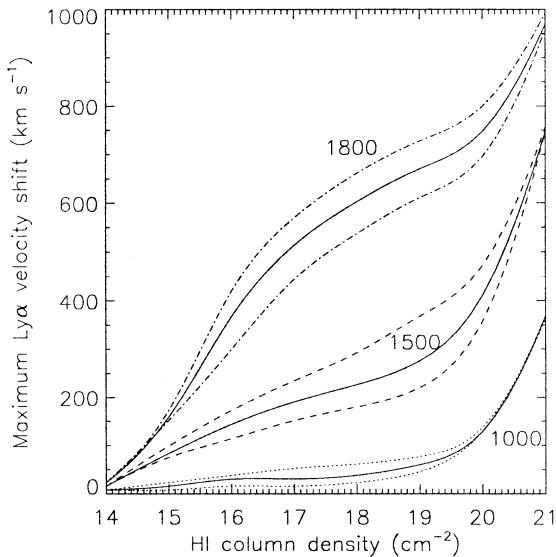


**Fig. 8.** Maximum velocity shifts of the peak of Ly $\alpha$  as a function of H I absorption column density. The solid lines are for the indicated original widths of Ly $\alpha$  emission (in units km s $^{-1}$  FWHM) and  $b = 50$  km s $^{-1}$ . Lower and upper dashed/dotted lines correspond to  $b = 25$  and  $b = 754$  km s $^{-1}$

## 5. Discussion

### 5.1. USS selection efficiency

The technique of selecting ultra steep spectrum radio sources, has proven to be very successful in finding distant radio galaxies. In total we have obtained spectra of 147 objects, of which for 64 (44%) we have been able to determine a redshift. From the remaining objects no clear emission lines were observed. There are four possible explanations for the failure to detect emission lines in these objects. First, the objects did not have emission lines of sufficient strength to be detectable in the given atmospheric conditions and sensitivities. Secondly, many of these sources may be at redshifts between  $\sim 1.2$  and  $\sim 1.6$ , where there are no extremely strong emission lines visible in the optical window. Thirdly, some objects may be at  $z > 5$ , where Ly $\alpha$  is shifted beyond the red of the window to be observable. Fourthly, there may have been some unseen errors in the telescope pointing. Of the 147 objects observed, 29 (19.7%) are at redshifts larger than 2, which shows that the USS selection is indeed an efficient way of finding very distant radio galaxies. Taking into account the preselections from VLA imaging of  $\sim 600$  sources and from  $R$  band CCD imaging of  $\sim 300$  objects, we can say that of the radio sources with spectral index  $\alpha < -1$ , radio size  $< 20''$  and faint optical identification ( $R > 21$ ), roughly 1 in 5 objects is at a redshift larger than 2.

To further assess the efficiency of the USS selection technique we examined the relation between redshift and spectral index. In Fig. 6 we plot this relation for a total of 108 radio galaxies, where the spectral index is that defined between the lowest available frequency above 150 MHz and 5 GHz. Apart from our USS sources (selected  $\alpha < -1$ ), this plot also includes

radio galaxies from the Molonglo Survey ( $\alpha < -0.9$ , McCarthy et al. 1990a, 1990b), the Bologna Radio catalogue ( $\alpha < -0.9$ , McCarthy et al. 1991; Lilly 1988), 8C (Lacy et al. 1994a; Lacy et al. 1992) and 6C (Eales et al. 1993a).

From this plot we see that there is a clear trend for the higher redshift sources to have steeper radio spectra. The median spectral index of all sources is  $-1.15$ . At  $z < 1$  the median spectral index is  $-1.08$ , at redshifts between 1 and 2 it is  $-1.16$ , at redshifts between 2 and 3 it is  $-1.19$  and at  $z > 3$  the median spectral index is  $-1.31$ . A Spearman Rank correlation analysis shows that the correlation between spectral index and redshift is present at a confidence level of more than 99.9%. If only considering the radio galaxies at redshifts larger than 1, this correlation is still significant at the 98% confidence level.

Particularly, for the steepest spectra the efficiency of the technique in finding the most radio distant radio galaxies is remarkable. Of all sources with radio spectra steeper than  $-1.3$  almost  $30\% \pm 15\%$  are at redshifts larger than 3, compared with only  $3\% \pm 2\%$  of the sources with spectral index between  $-0.9$  and  $-1.3$ .

This continued steepening of the observed radio spectra with redshift can be understood as the effects of the ‘‘K-correction’’ at radio wavelengths: There is a well known tendency of radio sources to have spectra which steepen at higher frequencies. For objects at higher redshifts the receivers sample higher emitted frequencies and steeper spectra. Evidence that the intrinsic radio spectra of HZRGs indeed continue to steepen to higher frequencies comes from 5 and 8 GHz VLA observations of our sample (Carilli et al. 1997). An additional effect that could contribute is that the radio emission would have an intrinsically steeper spectrum at a fixed rest frame frequency due to increased inverse Compton losses from scattering of the microwave background, which is stronger at higher redshifts (Krolik & Chen 1991; see also Blumenthal & Miley 1979; Chambers et al. 1990).

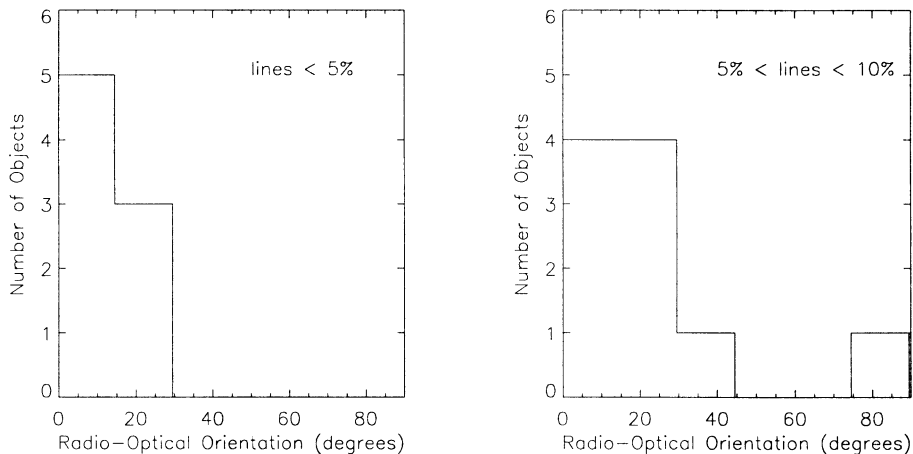
Further it has been suggested that the spectral index might be linked to the total radio power (Laing & Peacock 1980) possibly due to the density of the environment. Because we are observing a flux limited radio sample, the objects at the highest redshifts may have a larger average radio power. However, at  $z > 2$  the range in radio power of the sources is relatively small. There is no evidence for a correlation between radio power and the spectral index of the  $z > 2$  sources (see Carilli et al. 1997). Although a mechanism in which a denser environment of a radio source (as might be expected around primeval galaxies in the early Universe) may cause the radio lobes to have a steeper spectrum, the most plausible cause for the strong relation of spectral index with redshift, remains the steepening of the radio spectrum at higher rest frame frequencies with a possible contribution from increased inverse Compton losses due to the more intense microwave background at high redshifts.

### 5.2. The evolution of the space density of radio galaxies

Although there appears to be an abrupt decrease in the observed number of radio galaxies at redshifts  $z > 3$ , this does not necessarily imply a real decrease in the space density of radio galaxies

**Table 4.** Measured velocity shifts between emission lines

name	Velocity shifts (km s <sup>-1</sup> )					
	CIV-Ly $\alpha$	HeII-Ly $\alpha$	CIII]-Ly $\alpha$	CIV-HeII	CIV-CIII	HeII-CIII
0200+015	-185 ± 285	-83 ± 220	324 ± 226	-101 ± 257	-509 ± 263	-408 ± 190
0211-122	-528 ± 156	-315 ± 160	-53 ± 156	-213 ± 131	-474 ± 126	-261 ± 132
0214+183				-867 ± 265	-623 ± 149	245 ± 263
0355-037	-19 ± 325	221 ± 326	206 ± 233	-241 ± 386	-226 ± 312	14 ± 313
0417-181	298 ± 218	532 ± 185		-234 ± 190		
0748+134	295 ± 210	756 ± 326	811 ± 315	-461 ± 350	-516 ± 340	-55 ± 421
0857+036	-80 ± 177	503 ± 165		-583 ± 207		
0943-242	-62 ± 148	279 ± 96	551 ± 361	-341 ± 159	-614 ± 382	-273 ± 365
1138-262	-968 ± 433	465 ± 448	317 ± 1216	-1429 ± 562	-1281 ± 1262	148 ± 1268
1357+007	242 ± 295					
1410-001	-197 ± 115	-22 ± 152	330 ± 193	-174 ± 158	-527 ± 198	-353 ± 222
1545-234	227 ± 237	91 ± 250		135 ± 314		
1558-003	-599 ± 165	-194 ± 276	-431 ± 231	-403 ± 297	-168 ± 257	236 ± 339
1707+105		984 ± 195	734 ± 1063			251 ± 1071
2202+128	41 ± 294	690 ± 737		-648 ± 783		
2251-089				-482 ± 210	-582 ± 204	-100 ± 212
4C23.56				-443 ± 781	311 ± 612	754 ± 576
4C24.28	-1336 ± 1235					
4C28.58				362 ± 861	-626 ± 563	-990 ± 733
4C40.36				456 ± 355	457 ± 383	1 ± 333
4C41.17	-165 ± 573					
4C48.48				-302 ± 293	-743 ± 233	-441 ± 271
4C60.07	464 ± 564					

**Fig. 9.** Difference between the orientation of the optical  $R$  band and the radio axes for 18 USS sources with  $1.9 < z < 3$ . At these redshifts there are no strong emission lines with wavelength within the filter band-pass. The alignment is similarly strong for objects with line contaminations in  $R$  band of 5%–10% as for those objects with less than 5% line contamination

at those redshifts (e.g. Dunlop & Peacock 1990). A nice way to test for evolution beyond a defined redshift  $z_0$  is to use a modified version of the  $\langle V/V_{max} \rangle$  test, the “binned  $\langle V'/V'_{max} \rangle$ ” (e.g. Osmer & Smith 1980).

For such a test it is important that the flux limit of a survey is well established. The flux limits for our samples of USS sources are not well defined for three reasons. First, our sample from the Texas Catalogue and the sample from the 4C survey do not have a well determined flux limit. At low flux levels ( $< 0.5$  Jy for the Texas Catalogue and  $< 2$  Jy for 4C) the surveys are incomplete. Secondly, the actual flux limit for the Texas Catalogue is a function of source morphology. Thirdly, the selection on spectral index by combining two radio catalogues increases the flux limit at low frequencies for sources with steeper spectra.

This poorly known flux limit introduces an error in the  $\langle V'/V'_{max} \rangle$  of at least 0.1 – 0.2 (see Röttgering 1993). Therefore we conclude that our present sample of USS radio galaxies, does not allow us to decide whether there is a decrease in source density at the highest redshifts.

### 5.3. Ionization of the emission line gas

Three important ionization mechanisms that have been considered for the emission line regions of radio galaxies are shock ionization from the interaction with the radio lobes, photoionization by hot stars and photoionization by the active nucleus. In general, the line ratios of radio galaxies and the rest frame equivalent width of Ly $\alpha$  are not well reproduced by shock ionization

models, nor by hot stars, and photoionization by a nuclear UV continuum appears to be the dominant mechanism of ionization (Baum & Heckman 1989a, 1989b; Baum et al. 1992; McCarthy 1993; Ferland & Osterbrock 1986, 1987; Chambers et al. 1990; Charlou & Fall 1993).

The strong correlations between the equivalent width of the emission lines found for our sample is further support that the emission lines are all produced by the same ionization mechanism and are consistent with central photoionization.

#### 5.4. Velocity shifts: possible associated absorption systems

Velocity shifts between different emission lines in the spectrum of quasars occur frequently. For the broad lines of quasars, the high ionization lines and Ly $\alpha$  are systematically blueshifted with respect to the low ionization lines and H $\alpha$  by as much as 4000 km s<sup>-1</sup> (Gaskell 1982; Wilkes 1984; Espey et al. 1989; Corbin 1990; Carswell et al. 1991). These velocity shifts have been attributed to outflow of highly ionized gas from the active nucleus in combination with obscuration of the far side of the quasar's emission line region.

The characteristics of the velocity shifts in our HZRGs are quite different from those of quasars. Not only are the shifts generally smaller, but also the shifting of the peak of the Ly $\alpha$  line with respect to the peak of the higher ionization lines is not observed in quasars, where Ly $\alpha$  together with the higher ionization lines are shifted with respect to the lower ionization lines and H $\alpha$ . Furthermore, in quasars the shifts are observed in the broad line region, i.e. on a very different scale than the narrow line region of radio galaxies. It is therefore plausible that the origin of the velocity shifts between the emission lines in HZRGs is different from that in quasars.

We consider two explanations for the occurrence of the velocity shifts in our sample of HZRGs. First, the spatial distribution and the velocity field of the high ionization lines and the Ly $\alpha$  emission lines are not necessarily the same and could lead to the observed velocity shifts. In radio galaxies there have been reports of velocity shifts of up to  $\sim 1000$  km s<sup>-1</sup> between the emission lines (McCarthy et al. 1990a; Tadhunter 1991; Eales et al. 1993b). These have also been proposed to be related to the nuclear activity (Tadhunter 1991) or to be due to inflow or outflow on the near side of the galaxy, with obscuration of the emission from the far side of the galaxy (Eales et al. 1993b).

Secondly, a large fraction (60%) of HZRG show the presence of strong associated H I absorption in spectra of Ly $\alpha$  emission at a resolution a magnitude higher than the spectra presented in this paper (Röttgering et al. 1995; van Ojik et al. 1997). In most cases the Ly $\alpha$  emission is absorbed at wavelengths blueward of the peak of the Ly $\alpha$  emission, resulting in a red-shift of the peak of the Ly $\alpha$  emission when observed at low resolution.

Since the observed correlations appear to be mainly due to the Ly $\alpha$  emission line shifting with respect to the higher ionization lines, this indicates that H I absorption systems may play a role in producing the observed velocity shifts. In the next paragraph this will be further considered.

#### 5.4.1. Simulations of Ly $\alpha$ velocity shifts caused by H I absorption

Because of resonant scattering of Ly $\alpha$  photons, associated H I absorption systems can produce a strong absorption feature in the Ly $\alpha$  emission profile that alters the shape of the line. When observed at low spectral resolution this may result in a slightly different redshift for the Ly $\alpha$  line than for the higher ionization lines. An absorber located at a small blueshift (or redshift) with respect to Ly $\alpha$  will cause a slightly higher (or lower) redshift for the measured peak of Ly $\alpha$ . To investigate whether the effect of associated H I absorption systems on Ly $\alpha$  could indeed produce the range of observed velocity shifts, we have simulated the profile which would be observed if a Ly $\alpha$  emission line with associated H I absorption was observed at low spectral resolution.

We assume that the original emission line profile of Ly $\alpha$  is Gaussian. An absorption feature is produced in the emission line profile by convolving it with a Voigt profile for a given H I column density and offset velocity from the Ly $\alpha$  emission peak. The resultant theoretical profile of Ly $\alpha$  emission with absorption feature is then convolved with the instrumental resolution. The peak position of this simulated "observed" profile is determined and gives the offset velocity with respect to the peak of the original Gaussian Ly $\alpha$  emission line profile.

We have carried out the simulations for an instrumental spectral resolution of 20 Å (FWHM) which is representative for our observations, and an observing wavelength of 4000 Å for Ly $\alpha$ , so that the instrumental resolution is 1500 km s<sup>-1</sup>. The parameters that influence the resultant Ly $\alpha$  velocity shift are the offset velocity of the H I absorption system, the H I column density, the Doppler parameter ( $b$ ) of the absorber, and the width of the original Gaussian Ly $\alpha$  emission line. From the high resolution observations of 0943-242 (Röttgering et al. 1995) it was found that the H I absorption system has a column density of  $\sim 10^{19}$  cm<sup>-2</sup> with a Doppler parameter of 55 km s<sup>-1</sup>, while the velocity width of the original Ly $\alpha$  emission profile was estimated to be 1575 km s<sup>-1</sup>. The velocity width of Ly $\alpha$  is usually in the range of 1000–1500 km s<sup>-1</sup> (FWHM) (e.g. McCarthy 1993; see also Sect. 3 and van Ojik et al. 1997). Therefore, we shall assume similar parameters of the Ly $\alpha$  emission and H I absorption systems for our simulations.

Column densities range from  $10^{14}$  to  $10^{21}$  cm<sup>-2</sup>, Doppler parameters of the absorption systems range from 25–75 km s<sup>-1</sup> and the offset velocity of the absorber is varied from 0 to 1500 km s<sup>-1</sup>. We have performed the simulations for input Gaussian emission lines of widths 1800, 1500 and 1000 km s<sup>-1</sup> (FWHM).

Fig. 7 shows the resultant velocity shifts for the observed Ly $\alpha$  profile as a function of absorber offset. The solid lines are for column densities  $10^{17}$ ,  $10^{19}$  and  $10^{20}$  cm<sup>-2</sup> with  $b = 50$  km s<sup>-1</sup>. For each column density the lower and upper dashed/dotted lines indicate the shifts for  $b = 25$  and  $b = 75$  km s<sup>-1</sup>. The different plots are for Ly $\alpha$  velocity widths of 1800, 1500 and 1000 km s<sup>-1</sup> (FWHM). Fig. 7 also shows the amount of flux that remains after H I absorption as a function of absorber offset, for H I col-

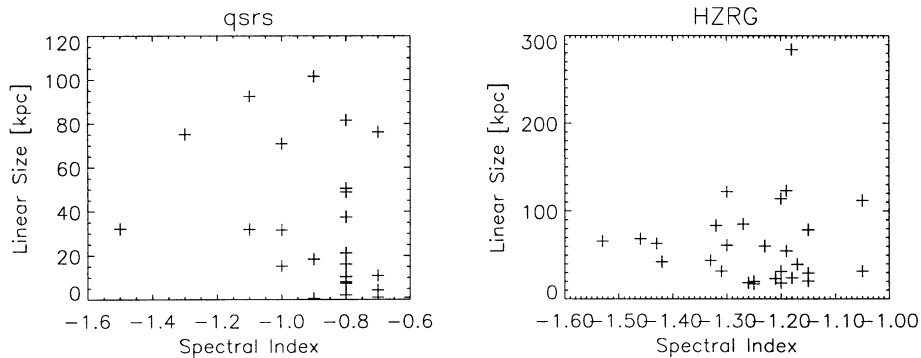


**Fig. 10.** Comparison of the projected linear sizes for  $z > 2$  radio sources. Left shows the steep spectrum quasars from the sample of Barthel and Miley. Right shows the distribution for our USS radio galaxies

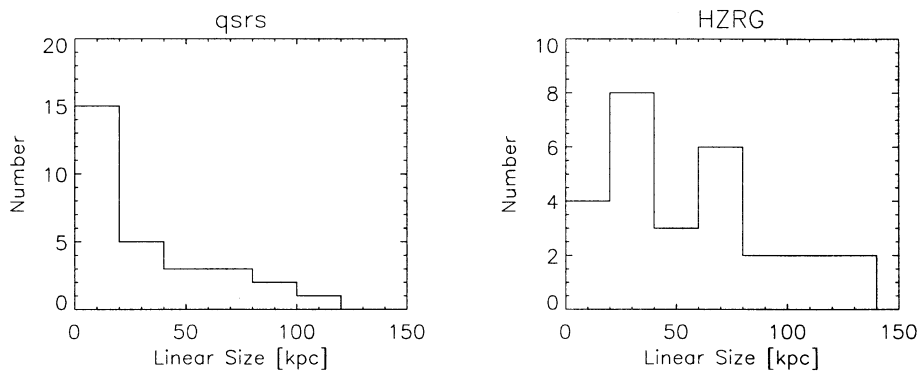


**Fig. 11.** The linear size as a function of spectral index for the  $z > 2$  USS radio galaxies (left) and quasars from the Barthel and Miley sample (right)

umn densities and  $\text{Ly}\alpha$  widths the same as above. The solid lines are for  $b = 50 \text{ km s}^{-1}$ , while lower and upper dotted lines now correspond to  $b = 75$  and  $b = 25 \text{ km s}^{-1}$ . Fig. 8 indicates the maximum shift of the  $\text{Ly}\alpha$  peak that can be produced by H I absorption systems of different column densities and Doppler parameters.

We find from these simulations that, depending on the velocity width of  $\text{Ly}\alpha$  emission line, H I absorption systems can produce velocity shifts in the observed peak of  $\text{Ly}\alpha$  emission of  $100\text{--}600 \text{ km s}^{-1}$  for H I column densities of  $10^{17} - 10^{20} \text{ cm}^{-2}$ . Such velocity shifts are comparable with the velocity shifts observed in our sample of radio galaxies. Thus, the velocity shifts between  $\text{Ly}\alpha$  and the higher ionization lines could be explained if the majority of HZRGs have strong ( $N(\text{H I}) \sim 10^{17} - 10^{20} \text{ cm}^{-2}$ ) associated absorption. However, the presence of associated H I absorption systems cannot be the cause for all observed velocity shifts between the various emission lines. Of the objects with significant velocity shifts, there are at least five with known strong H I absorption in the  $\text{Ly}\alpha$  line (van Ojik et al. 1997), but also four that do not have strong associated H I absorption. These last objects actually have some of the largest observed significant velocity shifts between the emission lines. Furthermore, the origin of the observed systematic shift of C IV with respect to He II and C III] is unclear. Possibly, different velocity profiles cause the observed shifts between these emission lines if they originate from different regions in the galaxies. We note that C IV is also sensitive to absorption. However, for an H I absorption with high column density ( $> 10^{18} \text{ cm}^{-2}$ ), the associated C IV absorption column density is usually a factor

$10^4 - 10^5$  lower (e.g. Bergeron & Stasińska 1988) and will not have a very strong effect on the position of the peak of the line.

Thus, H I absorption systems cannot be the only cause of velocity shifts. Additional mechanisms such as outflow or inflow combined with obscuration, as proposed for quasars, or radio source induced displacements must be important.

### 5.5. Continuum alignment of the $z > 1.9$ Leiden compendium

It is well known that the major axes of the optical continuum and the radio emission of radio galaxies at  $z > 0.8$  are aligned, while low redshift radio galaxies have a weak tendency to have the optical minor axis aligned with the radio axis (Chambers et al. 1987; McCarthy et al. 1987). Interpretations of the “alignment effect” include jet-induced star formation and scattering of anisotropically emitted nuclear continuum (Begelman & Cioffi 1989; Rees 1989; di Serego Alighieri et al. 1989; Tadhunter et al. 1992).

The  $R$  band continuum of many of the  $z > 0.8$  radio galaxies is contaminated by strong emission lines extended in the direction of the radio axis. Such strong extended emission lines might cause the alignment effect, which is often measured at the lowest flux levels of the extended emission. It has therefore been suggested that the observed alignment does not involve the optical continuum (e.g. Meisenheimer et al. 1994). At redshifts of  $\sim 1$ , the strong  $[\text{O II}]\lambda 3727$  emission line is in  $R$  band. This emission line is usually spatially extended in the direction of the radio axis (see McCarthy et al. 1991b). At redshifts between 1.9 and 3, however, there are no strong emission lines in  $R$  band.

The only significant emission line present in  $R$  band at these redshifts might be  $C\text{ III]}\lambda 1909$ . From the measured equivalent widths measured for our sample of HZRGs we deduce that  $C\text{ III]}$  contributes less than 10% to the  $R$  band flux and often less than 5%. Although  $C\text{ III]}$  may be slightly spatially resolved, it is very unlikely that it would cause a strong alignment.

For 18 of the  $z > 1.9$  objects of the Leiden USS compendium we have the radio position angle from 20 cm VLA maps (Röttgering et al. 1994) and an  $R$  band image from which we could reliably determine the optical position angle (Röttgering et al. 1996a). Fig. 9 shows the difference between the optical continuum axis and the radio axis for these 18 objects, divided into two groups with less than 5% line contamination in  $R$  band and with line contamination between 5% and 10%. The alignment is similarly strong for both subsets, indicating that the minor contamination by line emission from  $C\text{ III]}$  in  $R$  band does not play a role. This plot provides further evidence that the previously inferred alignment between the optical continuum of HZRGs and the radio structure is real.

## 6. Radio source sizes

The observed differences between steep spectrum quasars and radio galaxies have been explained as merely due to whether the radio source axis is more closely aligned with the line of sight (quasars) or in the plane of the sky (galaxies) (see Antonucci 1993 and references therein). Clearly this model predicts that the projected linear sizes of quasars should on average be smaller than that of radio galaxies. Barthel (1989) found that steep-spectrum quasars with  $0.5 < z < 1$  have sizes that are systematically smaller than radio galaxies with  $0.5 < z < 1$  by a factor 2.2, indicating a cone angle of  $\sim 45^\circ$  along which the quasar can be seen. Gopal-Krishna and Kulkarni (1992) have obtained a similar results for a sample of radio sources with  $0.1 < z < 2$ . At low redshift, it seems that there is a relative shortage of observed steep spectrum quasars (Kapahi 1990), indicating that the simple unification scheme with a fixed cone angle breaks down at low  $z$ .

We have compared the radio source size distribution for the  $z > 2$  USS radio galaxies presented here with the radio source sizes for the  $z > 2$  quasars from the quasar sample studied by Barthel and Miley (Barthel & Miley 1988) (see Fig. 10). In both cases the linear sizes have been calculated using a Hubble constant of  $H_0 = 75 \text{ km s}^{-1} \text{ Mpc}^{-1}$  and a deceleration parameter of  $q_0 = 0.5$ . The mean angular radio size of the quasars is  $18 \pm 6$  and of the USS radio galaxies  $40 \pm 7.5$  kpc. The ratio between the sizes is 2.2, the same factor as has been found for the lower redshift objects. Within the context of the model of Barthel, this would imply that the cone angle of  $\sim 45^\circ$  that had been found for the sources with  $0.5 < z < 1$  also holds at high redshift.

However, there are two selection effects. First, as we have pointed out previously, there is an angular size bias in the USS sample in favour of small radio angular sizes. Secondly, the radio galaxies all have been selected to have ultra-steep spectral indices, whereas the quasars form a proper flux limited sample with a median spectral index of  $-0.8$ . We show the projected

linear size of the radio galaxies and quasars as a function of spectral index in Fig. 11. This shows evidence that the steepest-spectrum quasars tend indeed to be the largest. Restricting the sample to USS quasars, the 4 remaining sources are too few for a meaning full statistical comparison with the USS radio galaxies.

We therefore conclude that the difference in the source size distribution for the  $z > 2$  USS radio galaxies and radio galaxies is merely tentative. A proper comparison between the sizes of radio galaxies and quasars should include data covering a similar range of spectral indices for each species.

## 7. Summary and conclusions

In this paper we have presented spectroscopic results for galaxies associated with 64 ultra steep spectrum radio sources. Of these radio galaxies, 29 are at  $z > 2$  and the three highest redshifts are 3.6, 3.8 and 3.8. Our ultra steep spectrum (USS) criterion ( $\alpha < -1$ ) has proven to be the most efficient way of finding distant radio galaxies. We find that even among the USS sources, there is a strong correlation between the spectral index and redshift. The most distant radio galaxies within the USS sample have the steepest radio spectra.

In our sample there are 3 radio galaxies at  $z > 3$  and 26 at  $2 < z < 3$ . However, the present sample of USS radio galaxies does not allow us to decide whether there is a decrease in co-moving source density at the highest redshifts, because of the uncertain flux limit of the sample of radio sources.

We have analyzed the spectra of the 30 objects with the highest redshifts ( $z > 1.9$ ). For these high redshift radio galaxies,  $\text{Ly}\alpha$  is almost always the dominant emission line, with a rest frame equivalent width ranging from  $\sim 100 \text{ \AA}$  to more than  $1000 \text{ \AA}$ . The equivalent widths of the most important emission lines ( $\text{Ly}\alpha$ ,  $C\text{ IV}$ ,  $\text{He II}$ ,  $C\text{ III]}$ ) are found to correlate strongly with each other. The large rest frame equivalent widths and the correlation between the equivalent widths of the emission lines, confirm that photoionization by a central continuum source is most likely the dominant ionization mechanism.

There are significant velocity differences between the various emission lines of our high redshift radio galaxies; mainly the  $\text{Ly}\alpha$  line is shifted with respect to the higher ionization lines. Velocity shifts range from 100 to almost  $1000 \text{ km s}^{-1}$  in some cases. Simulations show that the effects of associated  $\text{H I}$  absorption on the  $\text{Ly}\alpha$  emission line may be responsible for most of these velocity shifts. However, in at least a few objects, other mechanisms such as organized kinematics of the  $\text{Ly}\alpha$  emission line gas (e.g. inflow or outflow) and obscuration of the line emission from the far side of the galaxy must play a role.

The sample of objects discussed here is well suited for follow-up observations. Various detailed studies of their properties are presented in other papers or are underway, both with ground-based telescopes and with the HST.

*Acknowledgements.* We acknowledge support from an EU twinning project, funding from the high- $z$  programme subsidy granted by the Netherlands Organization for Scientific Research (NWO) and a NATO research grant. The work by WvB for this project was performed at

IGPP/LLNL under the auspices of the U.S. Dept. of Energy under contract W-7405-ENG-48.

## References

- Antonucci R., 1993, *ARA&A* 31, 473
- Barthel P.D., 1989, *ApJ* 336, 606
- Barthel P.D., Miley G.K., 1988, *Nat* 333, 319
- Baum S.A., Heckman T.M., 1989a, *ApJ* 336, 681
- Baum S.A., Heckman T.M., 1989b, *ApJ* 336, 702
- Baum S.A., Heckman T.M., van Breugel W., 1992, *ApJ* 389, 208
- Begelman M.C., Cioffi D.F., 1989, *ApJ* 345, L21
- Bergeron J., Stasińska G., 1986, *A&A* 169, 1
- Blumenthal G., Miley G., 1979, *A&A* 80, 13
- Carilli C.L., Röttgering, van Ojik R., H.J.A., Miley G.K., van Breugel W., 1997, *ApJsup* 109, 1
- Carswell R.F., Mountain C.M., Robertson D.J., et al., 1991, *ApJ* 381, L5
- Chambers K.C., Miley G., 1989, In: Kron, R.C. (ed.) *The Evolution of the Universe of Galaxies: The Edwin Hubble Centennial Symposium*. San Francisco: Astron. Society of the Pacific, p. 373
- Chambers K.C., Miley G., van Breugel W., 1988, *ApJ* 327, L47
- Chambers K.C., Miley G.K., van Breugel W., 1987, *Nat* 329, 604
- Chambers K.C., Miley G.K., van Breugel W.J.M., 1990, *ApJ* 363, 21
- Chambers K.C., Miley G.K., van Breugel W.J.M., Huang J., 1996a, *ApJsup* 106, 215
- Chambers K.C., Miley G.K., van Breugel W.J.M., M.A.R. Bremer, J.-S. Huang, N.A. Trentham, 1996b, *ApJsup* 106, 247
- Charlot S., Fall S.M., 1993, *ApJ* 415, 580
- Condon J., 1989, *ApJ* 338, 13
- Condon J., Broderick J., 1985, *AJ* 90, 2450
- Condon J., Broderick J., 1986, *AJ* 91, 1051
- Condon J., Broderick J., Seielstad G., 1989, *AJ* 97, 1064
- Corbin M.R., 1990, *ApJ* 357, 346
- di Serego Alighieri S., Fosbury R.A.E., Tadhunter P.Q.C., 1989, *Nat* 341, 307
- Douglas J.N., Bash F., Terrence G.W., Wolfe C., 1980, *The University of Texas Publications in Astronomy* 17, 1
- Dunlop J., Peacock J., 1990, *MNRAS* 247, 19
- Eales S.A., Rawlings S., Dickinson M., et al., 1993a, *ApJ* 409, 578
- Eales S.A., Rawlings S., Puxley P., Rocca-Volmerange B., Kuntz K., 1993b, *Nat* 363, 140
- Espey B.R., Carswell R.F., Bailey J.A., Smith M.C., Ward M.J., 1989, *ApJ* 342, 666
- Fanaroff B.L., Riley J.M., 1974, *MNRAS* 167, 31
- Ferland G., Osterbrock D., 1986, *ApJ* 300, 658
- Ferland G., Osterbrock D., 1987, *ApJ* 318, 145
- Gaskell C.M., 1982, *ApJ* 263, 79
- Gopal-Krishna, Kulkarni V.K., 1982, *A&A* 257, 11
- Hales S.E.G., Baldwin J.E., Warner P.J., 1988, *MNRAS* 234, 919
- Heckman T.M., Lehnert M.D., Miley G.K., van Breugel W., 1991, *ApJ* 381, 373
- Heckman T.M., van Breugel W.J.M., Balick B., Butcher H.R., 1982, *ApJ* 262, 529
- Kapahi V.K., 1990, In: Zensus J.A., Pearson T.J. (eds.) *Parsec-Scale Radio Jets*. p. 397
- Krolik J.H., Chen W., 1991, *AJ* 102, 1659
- Lacy M., Miley G., Rawlings S., et al., 1994a, *MNRAS* 271, 504
- Lacy M., Rawlings S., Warner P.J., 1992, *MNRAS* 256, 404
- Laing R., Peacock J.A., 1980, *MNRAS* 190, 903
- Large M.I., Mills B.Y., Little A.C., Crawford D.F., Sutton J.M., 1981, *MNRAS* 194, 693
- Lilly S., 1988, *ApJ* 333, 161
- McCarthy P.J., van Breugel W., Kapahi V.K., 1991, *ApJ* 371, 478
- McCarthy P., 1991, *AJ* 102, 518
- McCarthy P., Spinrad H., van Breugel W., et al., 1990a, *ApJ* 365, 487
- McCarthy P., van Breugel W., Spinrad H., Djorgovski S., 1987, *ApJ* 321, L29
- McCarthy P.J., 1993, *ARA&A* 31, 639
- McCarthy P.J., Kapahi V.K., van Breugel W., Subrahmanya C., 1990b, *AJ* 1014, 100
- Meiseneimer K., Hippelein H., Neeser M., 1994, In: Bicknell G.V., Dopita M.A., Quinn P.J. (eds.) *The First Stromlo Conference: The Physics of Active Galaxies*. Vol. 54, p. 397
- Miley G., Chambers K., 1989, In: Meurs E.J.A., Fosbury R.A.E. (eds.) *ESO Workshop on Extranuclear Activity in Galaxies*, p. 43
- Osmer P.S., Smith M.G., 1980, *ApJS* 42, 333
- Osterbrock D.E., 1989, *Astrophysics of Gaseous Nebulae and Active Galactic Nuclei*, Mill Valley: University Science Books
- Pentericci L., Röttgering H.J.A., Miley G.K., Carilli C.L., McCarty P., 1997, in press
- Rees M.J., 1989, *MNRAS* 239, 1P
- Rees N., 1990, *MNRAS* 244, 233
- Röttgering H.J.A., 1993, Ph.D. thesis, University of Leiden
- Röttgering H.J.A., Lacy M., Miley G.K., Chambers K.C., Saunders R., 1994, *A&AS* 108, 79
- Röttgering H.J.A., Hunstead R., Miley G.K., van Ojik R., Wieringa M.H., 1995, *MNRAS* 277, 389
- Röttgering H.J.A., Miley G.K., Chambers K.C., 1996a, *A&AS* 114, 51
- Röttgering H.J.A., West M.J., Miley G.K., Chambers K.C., 1996b, *A&A* 307, 376
- Spinrad H., 1986, *PASP* 98, 601
- Tadhunter C.N., 1991, *MNRAS* 251, 46P
- Tadhunter C.N., Scarrott S., Draper P., Rolph C., 1992, *MNRAS* 256, 53p
- Tielens A., Miley G., Willis A., 1979, *A&AS* 35, 153
- van Breugel W.J.M., Miley G.K., Heckman T.M., Butcher H., Bridle A., 1985, *ApJ* 290, 496
- van Ojik R., Röttgering H.J.A., Carilli C., Miley G.K., Bremer M.N., Macchetto F., 1996, *A&A* 313, 25
- van Ojik R., Röttgering H.J.A., Miley G.K., Hunstead R.W., 1997, *A&A* 317, 358
- Wilkes B.J., 1984, *MNRAS* 207, 73